NATIONAL ADVISORY COMMITTEE FOR AERONAUTICS

TECHNICAL NOTE 2819

EFFECT OF HIGH-LIFT DEVICES ON THE STATIC-LATERAL-STABILITY DERIVATIVES OF A 45° SWEPTBACK WING OF ASPECT RATIO 4.0 AND TAPER RATIO 0.6 IN COMBINATION WITH A BODY

By Jacob H. Lichtenstein and James L. Williams

Langley Aeronautical Laboratory
Langley Field, Va.

Washington

November 1952

1A

NATIONAL ADVISORY COMMITTEE FOR AERONAUTICS

TECHNICAL NOTE 2819

EFFECT OF HIGH-LIFT DEVICES ON THE STATIC-LATERAL-STABILITY DERIVATIVES OF A 45° SWEPTBACK WING OF ASPECT RATIO 4.0 AND TAPER RATIO 0.6 IN COMBINATION WITH A BODY

By Jacob H. Lichtenstein and James L. Williams

SUMMARY

An investigation has been made in the Langley stability tunnel to determine the effect of high-lift devices on the low-speed static-lateral-stability derivatives of a 45° sweptback wing of aspect ratio 4.0 and taper ratio 0.6. Comparison between the increments in the static-lateral-stability derivatives due to flap deflection obtained from experiment and the increments evaluated by a simple sweep theory is also made.

The results of the investigation show that, for moderate and high-lift coefficients, an increase in trailing-edge flap span, with or without a leading-edge slat, generally resulted in increased effective dihedral and directional stability. The leading-edge slats tended mainly to extend the trends obtained at low lift coefficients for the dihedral effect to nearer maximum lift. An application of simple sweep theory and measured lift and drag increments to the evaluation of the increments in the static-lateral-stability derivatives due to trailing-edge flaps indicates that the trend and approximate magnitude of the variation of these increments with flap span are predicted in the moderate and high lift-coefficient range.

INTRODUCTION

Requirements for satisfactory high-speed performance of aircraft have resulted in configurations that differ in many respects from previous designs. As a result of these changes, the designer has little assurance that the low-speed characteristics will be satisfactory for any specific configuration. The low-speed characteristics of wings suitable for high-speed flight and the effect of high-lift devices on static longitudinal characteristics of these wings have already been investigated extensively. There is, however, only meager published information on the effect of high-lift devices on the static lateral

stability characteristics of such wings. In order to provide additional information on this subject, an investigation of the effect of high-lift devices on the static lateral stability characteristics of wings suitable for high-speed flight is being made in the Langley stability tunnel. This investigation is part of a general program being conducted in the Langley stability tunnel to determine the effect of arbitrary changes in configuration on the stability characteristics of typical airplane models. The present investigation is concerned with the effect of high-lift devices on the static lateral stability characteristics of a swept-wing—body configuration. The high-lift devices consisted of plain and split trailing-edge flaps of various spans employed with and without full-span leading-edge slats.

The model used in the present investigation had a 45° sweptback wing of aspect ratio 4 and taper ratio 0.6. The model was similar to that used previously in an investigation of the effects of vertical-tail size and length on the static lateral and yawing characteristics of an airplane model (refs. 1 and 2).

SYMBOLS

The results of the tests are presented as standard NACA coefficients of forces and moments which are referred to the stability axes system with the origin at the projection on the plane of symmetry of the quarter-chord point of the mean aerodynamic chord of the wing. The positive directions of the forces, moments, and angular displacements are shown in figure 1. The coefficients and symbols are defined as follows:

C_L lift coefficient, $\frac{\text{Lift}}{qS_W}$

C_D drag coefficient, $\frac{\text{Drag}}{qS_W}$

C_{D_o} profile drag coefficient, $C_D - \frac{C_L^2}{\pi A}$

C_Y lateral-force coefficient, $\frac{\text{Lateral force}}{qS_W}$

C_l rolling-moment coefficient, $\frac{\text{Rolling moment}}{qS_W b}$

C_n yawing-moment coefficient, $\frac{\text{Yawing moment}}{qS_W b}$

C_m pitching-moment coefficient, $\frac{\text{Pitching moment}}{qS_W\bar{c}}$

$C_{L_{max}}$ maximum C_L for the specific configuration

C_1 primary force coefficient, $\frac{G_1}{qS_W}$

C_2 primary force coefficient, $\frac{G_2}{qS_W}$

G_1 component of resultant semispan load directed normal to plane formed by velocity vectors V and V_n (see fig. 13), lb

G_2 component of resultant semispan load directed parallel to V_n (see fig. 13), lb

q dynamic pressure, $\frac{1}{2}\rho V^2$, lb/sq ft

ρ mass density of air, slugs/cu ft

V free-stream velocity, ft/sec

V_n component of free-stream velocity normal to wing quarter-chord line, ft/sec

V_s component of free-stream velocity parallel to wing quarter-chord line, ft/sec

S_W wing area, sq ft

S_f area of wing within flap span, sq ft

b wing span, perpendicular to plane of symmetry, ft

b_s slat span, perpendicular to plane of symmetry, ft

y_f flap semispan, measured from and perpendicular to plane of symmetry, ft

y_W lateral distance perpendicular to plane of symmetry, ft

y_{L_W} effective lateral center of pressure of wing lift load perpendicular to plane of symmetry, ft

y_{L_f} effective lateral center of pressure of increment in lift due to flap deflection, perpendicular to plane of symmetry, ft

y_{D_f} effective lateral center of pressure of increment in drag due to flap deflection, perpendicular to plane of symmetry, ft

c chord of wing, measured parallel to plane of symmetry, ft

$\bar{c}$ mean aerodynamic chord, $\frac{2}{S_W}\int_0^{b/2} c^2\, dy_W$; measured parallel to plane of symmetry, ft

$\bar{c}'$ mean chord, $\frac{S_W}{b}$; measured parallel to plane of symmetry, ft

c_s chord of slat, measured parallel to plane of symmetry, ft

c_f chord of flap, measured parallel to plane of symmetry, ft

$\bar{x}$ longitudinal distance rearward from airplane center of gravity to wing aerodynamic center, ft

x_{L_f} longitudinal distance forward from wing aerodynamic center to center of pressure of lift load due to flap deflection, ft

x_{D_f} longitudinal distance forward from wing aerodynamic center to center of pressure of drag load due to flap deflection, ft

A aspect ratio, $\frac{b^2}{S_W}$

A' effective aspect ratio of flapped part of wing, $A\frac{y_f}{b/2}$

λ taper ratio, ratio of tip chord to root chord

Λ angle of sweep, positive for sweepback, deg

Λ_h angle of sweep of flap hinge line, positive for sweepback, deg

α angle of attack, measured in plane of symmetry, deg

α_i induced angle of attack

β angle of sideslip, deg

δ flap deflection relative to wing, positive when trailing edge is down, measured in plane normal to hinge line, deg

a_o section lift-curve slope when placed normal to air stream

c_l section lift coefficient

α_δ flap-effectiveness parameter, measured in plane normal to hinge line

$C_{Y_\beta} = \frac{\partial C_Y}{\partial \beta}$

$C_{n_\beta} = \frac{\partial C_n}{\partial \beta}$

$C_{l_\beta} = \frac{\partial C_l}{\partial \beta}$

ΔC_{l_β}, ΔC_{n_β}, ΔC_{Y_β} increment in C_{l_β}, C_{n_β}, C_{Y_β} due to flap deflection at constant α or C_L (for example, $(C_{l_\beta})_{\text{wing with flaps}} - (C_{l_\beta})_{\text{wing without flaps}}$)

ΔC_{L_f} increment in lift coefficient due to flap deflection at a specific angle of attack

ΔC_{D_o} increment in profile drag coefficient due to flap deflection $\left((C_{D_o})_{\text{with flaps}} - (C_{D_o})_{\text{without flaps}}\right)$

Subscripts:

L left semispan of wing, retreating semispan for positive sideslip

R right semispan of wing, advancing semispan for positive sideslip

MODEL-COMPONENT DESIGNATIONS

The components for the various configurations used in the present investigation are identified herein by the following letter designations:

W wing alone

WB wing-body configuration

S	slat
F_1	plain flap with outboard end at 0.4b/2
F_2	plain flap with outboard end at 0.7b/2
F_3	plain flap with outboard end at 1.0b/2
F_4	split flap with outboard end at 0.4b/2
F_5	split flap with outboard end at 0.7b/2
F_6	split flap with outboard end at 1.0b/2

MODEL, APPARATUS, AND TESTS

The general research model used for the present investigation was designed to permit tests of the wing-body configuration alone or with any of various combinations of slats and trailing-edge flaps. A sketch of the complete model is presented in figure 2, and a list of pertinent geometric characteristics of the various component parts is given in table I.

The wing had 45° sweepback of the quarter-chord line, an aspect ratio of 4.0, a taper ratio of 0.6, and NACA 65A008 airfoil sections parallel to the plane of symmetry. The ordinates for the NACA 65A008 airfoil section are given in table II. The wing was mounted along the body center line. The body was a body of revolution with a fineness ratio of 6.67. The body profile followed a circular arc over the front half and was faired to a blunt trailing edge over the rear half. Ordinates for the body profile are given in table III.

The high-lift devices used in the tests consisted of slats and plain and split trailing-edge flaps. The slats were of full span with a chord of 10 percent of the wing chord. This configuration was arbitrarily chosen to give increments in lateral stability with no attempt made to obtain optimum longitudinal stability. The ordinates of the slat are given in table IV and the slat-extension data are presented in figure 2. The chords of both the split and plain trailing-edge flaps were 20 percent of the wing chord. Three spans were used for both types of flaps which extended from the wing-body juncture to stations 40 and 70 percent of the wing semispan and to the wing tip. The deflection of the two types of flaps differed in that the split flap was deflected 60° from the lower surface or 54.6° from the chord plane, whereas the plain flap was deflected 40° from the chord plane. All parts of the model except the slats were constructed of mahogany. The slats were constructed

of metal to insure sufficient strength because of their thin section. A complete list of the configurations investigated is presented in table V.

The model was rigidly mounted on a single-strut support at the quarter-chord point of the wing mean aerodynamic chord which coincided with the midpoint of the body length. Forces and moments were measured by means of a conventional six-component-balance system. Photographs of the model as mounted in the tunnel for testing are presented in figure 3.

The tests of the present investigation were made in the 6- by 6-foot test section of the Langley stability tunnel. The dynamic pressure for the tests was 39.7 pounds per square foot, which corresponds to a Mach number of 0.16 and to a Reynolds number of 0.89×10^6 based on the wing mean aerodynamic chord. The angle of attack was varied from -6° to 24° and the angle of sideslip from about 5° to -5°.

CORRECTIONS

Approximate jet-boundary corrections based on unswept-wing concepts were applied to the angle of attack, drag coefficient, and rolling-moment coefficient. The dynamic pressure and drag coefficient were corrected for blocking effects by the methods presented in reference 3. The data have not been corrected for turbulence or support-strut interference, inasmuch as these effects are believed to be negligible for the parameters with which this paper is concerned.

RESULTS AND DISCUSSION

Presentation of Results

The basic data obtained in this investigation are presented in figures 4 to 8. A plot of $C_D - \frac{C_L^2}{\pi A}$ against α for the wing-body configuration and wing-body configuration with slats is presented in figure 9. A comparison of the measured increments in the static-lateral-stability derivatives due to flap deflection and calculated increments are presented in figure 10 for the wing used in the present tests. In addition, similar comparisons are made for the wing of reference 4 in figure 11 and for the sweptback wing of reference 5 in figure 12.

Longitudinal Stability Characteristics

The static-longitudinal-stability data are presented in figures 4 to 7. Inasmuch as the results for the wing-body configuration are very similar to those presented in reference 6 where the analysis of the results is adequately covered, they are not discussed in this paper.

For those configurations without slats (figs. 4 and 5), deflection of trailing-edge flaps, either plain or split, did not appreciably change the longitudinal stability characteristics from those obtained for the wing-body configuration alone up to about 0.75 maximum lift coefficient, although the change in trim was as expected. The severity of the instability which occurred just prior to the stall for the wing-body configuration, however, became greater as the flap span was increased. With the leading-edge slats extended (figs. 6 and 7), deflecting the trailing-edge flaps had a slight beneficial effect on the longitudinal stability characteristics.

In order to interpret data of configurations including a wing, consideration must be given to the angle-of-attack range over which the flow does not separate from the wing. As pointed out in reference 7, an indication of the limit of this range can be obtained by locating the initial break in the plot of $C_D - \frac{C_L^2}{\pi A}$ against angle of attack. A plot of this parameter is presented in figure 9 for the wing-body configuration and the wing-body configuration with slats extended. The curve for the wing-body configuration without slats initially breaks at about 6°; whereas, with the slat extended, the initial break is delayed until about 14°. For the wing-body configuration without slats, corresponding breaks were found in the C_L, C_m, and C_{l_β} curves. No such breaks were found for the configurations with slat extended. Inasmuch as tares were not taken into account, the absolute values of the drag coefficients should not be considered as representative of free-air values. The increments in drag coefficient due to flap deflection and the variation of drag with lift, however, should be reasonably accurate.

Although the increments in lift due to flap deflection for the plain flap were equal to or greater than those for the split flap, the increments in drag were somewhat less for the plain flap than for the split flap. The lift-drag ratio, therefore, for a given lift coefficient was higher for the plain flap than for the split flap, either with or without the slat.

Static Lateral Stability Characteristics

The static lateral stability characteristics for the wing-body combination with plain and split flaps both with and without leading-edge slats are presented in figure 8.

For the configurations without slats, the effect of flap deflection on C_{l_β}, C_{n_β}, and C_{Y_β} is generally similar to the effects found previously in reference 4. As discussed in reference 4, the short-span flap shifts the center of pressure inward from its position without flaps; consequently the C_{l_β} curve is shifted in a positive direction. Increasing the flap span generally shifts the curves in a negative direction because the center of pressure is moved outward from its position with short-span flaps. In addition, the flaps delay the positive break in the C_{l_β} curve until higher lift coefficients are attained so that at high lift coefficients the value of C_{l_β} becomes more negative for all the configurations with flaps than for the configuration without flaps.

The value of $C_{n_\beta} = -0.001$ for the wing-body configuration is in good agreement with the results presented in reference 6 for this configuration, and this instability is entirely due to the unstable moment of the body. Increasing the flap span generally tended to make C_{n_β} less negative (decreasing the directional instability) particularly at the higher lift coefficients. As a matter of fact, at about 0.9 maximum lift coefficient, the instability introduced by the body was nearly removed by the largest-span plain flap and fully removed by the largest-span split flap.

Addition of full-span leading-edge slats to the various configurations with and without trailing-edge flaps (figs. 8(c) and 8(d)) generally extended the trends of the C_{l_β} and C_{Y_β} curves obtained at low lift coefficients to higher lift coefficients. However, the slats generally introduce a slightly stable variation of C_{n_β} with increasing lift coefficients until the final break occurs just before maximum lift. The shifts in the values of C_{l_β} due to trailing-edge-flap deflection were similar in nature but of different magnitude with slats added to the wing as compared to the wing without slats (compare figs. 8(c) and 8(d) with 8(a) and 8(b)). Although the slats generally decreased the slope of C_{l_β} against C_L, they extended the linear part of the curve to nearly maximum lift, and, therefore, the maximum values of C_{l_β} were greater negatively (greater dihedral effect) with slats than without

the slats. The effect of flap span on C_{n_β} was less definite with the slats than without the slats.

The increments in C_{l_β}, C_{n_β}, and C_{Y_β} due to flap deflection at several lift coefficients are plotted against flap span for the various configurations in figure 10. The data show that for a selected value of lift coefficient ΔC_{l_β} became more negative as the flap span increased (fig. 10(a)). In general ΔC_{n_β} also increased slightly with increasing flap span (fig. 10(b)). At any flap span, ΔC_{n_β} varied erratically with lift up to about $0.9C_{L_{max}}$. At this value of C_L, ΔC_{n_β} was almost always greatest.

With the slat extended, the increments in C_{l_β} or C_{n_β} due to deflection of either the split or plain trailing-edge flap were smaller generally than the increment obtained when the respective flaps were deflected with the slat closed. With the slat extended, the increments in C_{l_β} or C_{n_β} were smaller when the plain flaps were deflected than when the split flaps were deflected. The larger displacement obtained when the split flaps were installed, as compared with that obtained with the plain flaps with or without the slats, could be due to the fact that the split flaps were deflected to a larger angle. (See fig. 2.)

Comparison of Calculated and Measured Values

In order to estimate the effect of flaps on the static lateral stability at an early stage in the design of swept-wing aircraft, theoretical expressions for the increments in C_{l_β}, C_{n_β}, and C_{Y_β} due to flap deflection $\left(\Delta C_{l_\beta}, \Delta C_{n_\beta}, \text{ and } \Delta C_{Y_\beta}\right)$ have been developed. A simple sweep theory similar to that which is used in reference 8 to develop stability derivatives for a wing alone was used herein with the additional simplification that the increments in load due to flap deflection are concentrated at the respective centers of pressure of the loads. The spanwise shift of the centers of pressure due to the presence of the body were not taken into account in developing these expressions. Since the same simple sweep theory was used herein as was used in reference 8, it is subject to the same limitations. The calculated results, therefore, indicate the trends and only the approximate magnitude of the effects of the flaps on the static-lateral-stability derivatives. Because of the assumptions made in the development of the theory, the accuracy decreases rapidly below a flap span of $0.4b/2$ and this circumstance should be borne in mind when these results are applied to such short flap spans. The formulas obtained for the increments in the

stability derivatives due to flap deflection are:

$$\Delta C_{l_\beta} = -\frac{\Delta C_{L_f}}{2}\frac{A' + 2\cos\Lambda}{A' + 4\cos\Lambda}(\tan\Lambda + \tan\Lambda_h)\frac{y_{L_f}}{b/2} \tag{1}$$

$$\Delta C_{n_\beta} = \frac{2(\Delta C_{L_f})^2}{\pi A' \frac{S_f}{S_W}\cos\Lambda}\left[\frac{A' + 2\cos\Lambda}{A' + 4\cos\Lambda}(\tan\Lambda + \tan\Lambda_h) - \frac{3\tan\Lambda}{2}\right]\left(\frac{\sin\Lambda}{A}\frac{\bar{x} - x_{L_f}}{\bar{c}'} + \frac{\cos\Lambda}{2}\frac{y_{L_f}}{b/2}\right) + \Delta C_{D_o}\left(\frac{\bar{x}' - x_{D_f}}{A\bar{c}'} + \tan\Lambda_h\frac{y_{D_f}}{b/2}\right) \tag{2}$$

$$\Delta C_{Y_\beta} = \frac{2(\Delta C_{L_f})^2}{\pi A' \frac{S_f}{S_W}}\tan\Lambda\left[\frac{3\tan\Lambda}{2} - \frac{A' + 2\cos\Lambda}{A' + 4\cos\Lambda}(\tan\Lambda + \tan\Lambda_h)\right] - \Delta C_{D_o} \tag{3}$$

A full development of these formulas is given in the appendix. The total stability derivative for a flapped wing is obtained by adding the increment to the value for the wing alone at the angle of attack under consideration.

The values of ΔC_{l_β}, ΔC_{n_β}, and ΔC_{Y_β} obtained by the use of these formulas in combination with the experimental values of ΔC_{L_f} and ΔC_{D_o} for the wing used for the present tests are presented in figure 10 for values of $C_L = 0.5$, $0.75C_{L_{max}}$, and $0.9C_{L_{max}}$. Both experimental and calculated values of ΔC_{l_β}, ΔC_{n_β}, and ΔC_{Y_β} are presented at lift coefficients of $0.75C_{L_{max}}$ and $0.9C_{L_{max}}$ for the wing of reference 4 ($A = 2.61$, $\Lambda = 45^\circ$, $\lambda = 1$) in figure 11, and for the sweptback wing of reference 5 ($A = 5$, $\Lambda = 35^\circ$, $\lambda = 0.5$) in figure 12. For the comparisons at $0.75C_{L_{max}}$ and $0.9C_{L_{max}}$, the values for the wing with flaps at $0.75C_{L_{max}}$ and $0.9C_{L_{max}}$ were compared with the values for the wing without flaps at $0.75C_{L_{max}}$ and $0.9C_{L_{max}}$. A comparison between the calculated and experimental values in figures 10, 11, and 12 shows that, in general, the proper variation of the stability derivatives with flap span and the approximate magnitude of the values of the stability derivatives are predicted by the theory.

The elementary considerations employed in this analysis, however, because of the exclusion of such items as separation and chordwise loading, do not appear to be sufficiently rigorous for an exact solution to problems of this nature.

CONCLUSIONS

The results of an investigation to determine the effect of trailing-edge-flap span on the static lateral stability characteristics of a 45° sweptback-wing—body configuration with and without full-span leading-edge slats indicate the following conclusions:

1. At moderate and high lift coefficients, an increase in trailing-edge flap span, with or without leading-edge slats, generally increased the effective dihedral and the directional stability.

2. The leading-edge slats tended to extend the trends obtained at low lift coefficients for the dihedral effect to nearer maximum lift.

3. An application of simple sweep theory, together with experimental lift and drag increments, to the evaluation of the increments in the static-lateral-stability derivatives due to trailing-edge flaps indicates that the trend and approximate magnitude of the variation of these increments with flap span are predicted by the theory in the moderate and high lift-coefficient range.

Langley Aeronautical Laboratory,
National Advisory Committee for Aeronautics,
Langley Field, Va., August 29, 1952.

APPENDIX

INCREMENTS IN STATIC-LATERAL-STABILITY DERIVATIVES DUE TO TRAILING-EDGE FLAP DEFLECTION FOR SWEPT WINGS

In the development of the formulas for evaluating the increments in the static-lateral-stability derivatives $(\Delta C_{l_\beta}, \Delta C_{n_\beta}$, and $\Delta C_{Y_\beta})$ due to trailing-edge flap deflection, the incremental lift ΔC_{L_f} and profile drag ΔC_{D_o} coefficients for the particular wing under consideration are assumed to be available from experimental data for use in the formulas. The derivatives presented herein are in the form of increments to be added to the wing-alone values at the angle of attack for which they were computed.

The method used herein consists of evaluating the loads due to flap deflection with approximate consideration given to the effects of aerodynamic induction on each of the wing semispans. The location and orientation of forces due to flap deflection used in this analysis are shown in figure 13. The magnitude and orientation of the semispan loads under sideslipping flight give rise to the stability derivatives. It is realized that increments probably exist in the stability derivatives of unswept wings due to flap deflection which also should be included, but the means for their evaluation is not readily apparent.

Centers of Pressure of Incremental Flap Load

For the purpose of determining the flap-load centers of pressure, the wing is assumed to be at zero angle of attack (zero wing lift) where the entire load is due to flap deflection. The spanwise shift in the centers of pressure of the load that would result from the presence of a body was not taken into consideration. Experiment has shown that for a wing with flaps, the loading of the wing is high over the flapped part of the wing and that, outboard of the flap, the loading drops rapidly to zero at the tip. In this analysis, the loading is assumed constant over the flapped part of the wing and is assumed triangular outboard of the flaps with the maximum value varying directly with the flap span. (See fig. 14.) Comparison of the derivatives calculated by using the span loading obtained from lifting-line theory and the assumed span loading for several cases indicated that the difference between the derivatives was within the accuracy of the theory. The flap chord was selected as 20 percent of the wing chord, and the flap load was assumed to act at the 50-percent-chord line of the wing. The incremental profile

drag was assumed uniform across the flap span. The effect of taper was taken into account in the expression for the lift and drag centers of pressure which in this analysis depend only upon flap span and taper. The span-load distribution of a wing with flaps indicates that, for the purpose of determining the aerodynamic induction, the effective aspect ratio of the flapped part of the wing A' should be used rather than the aspect ratio of the wing.

Expressions for the centers of pressure of the flap loads are

$$\frac{y_{L_f}}{b/2} = \frac{1}{2} \frac{1 + \lambda + (7 + \lambda)\frac{y_f}{b/2} - (9 - 5\lambda)\left(\frac{y_f}{b/2}\right)^2 + 3(1 - \lambda)\left(\frac{y_f}{b/2}\right)^3}{8 + \lambda - (7 - 4\lambda)\frac{y_f}{b/2} + 2(1 - \lambda)\left(\frac{y_f}{b/2}\right)^2}$$

$$\frac{y_{L_W}}{b/2} = \frac{1}{3} \frac{1 + 2\lambda}{1 + \lambda}$$

$$\frac{y_{D_f}}{b/2} = \frac{\frac{1}{2}\frac{y_f}{b/2} - \frac{1 - \lambda}{3}\left(\frac{y_f}{b/2}\right)^2}{1 - \frac{1 - \lambda}{2}\frac{y_f}{b/2}}$$

$$\frac{x_{L_f}}{\bar{c}'} = \frac{A \tan \Lambda}{6} \frac{1 + 2\lambda}{1 + \lambda} - \frac{y_{L_f}}{b/2}\left[\frac{0.5(\lambda - 1)}{1 + \lambda} + \frac{A \tan \Lambda}{2}\right] - \frac{0.5}{1 + \lambda}$$

$$\frac{x_{D_f}}{\bar{c}'} = \frac{A \tan \Lambda}{6} \frac{1 + 2\lambda}{1 + \lambda} - \frac{y_{D_f}}{b/2}\left(\frac{A \tan \Lambda}{2} - 1.3\frac{1 - \lambda}{1 + \lambda}\right) - \frac{1.3}{1 + \lambda}$$

Sideslipping Flight

In sideslipping flight for a constant-chord swept wing, the span-load distribution is considered, for this analysis, to be the same on both wing semispans although the magnitudes are different. The loads are affected by sideslip because of the manner in which sideslip affects

the velocities normal to the quarter-chord line. In sideslipping flight, the leading semispan (right semispan in this analysis) has less effective sweepback, whereas the trailing semispan (left semispan) has greater effective sweepback. The velocity component on the left semispan is altered, therefore, by the factor $\frac{\cos(\Lambda + \beta)}{\cos \Lambda}$. For a flapped wing of infinite span, the increment in lift due to sideslip on the left semispan can, therefore, be expressed as

$$\Delta c_{l_L} = \Delta c_{l_{\beta=0^\circ}} \left[\frac{\cos(\Lambda + \beta)\cos(\Lambda_h + \beta)}{\cos \Lambda \cos \Lambda_h} - 1 \right]$$

Inasmuch as

$$\Delta c_{l_{\beta=0^\circ}} = a_o \alpha_\delta \delta \cos \Lambda \cos \Lambda_h = \Delta c_{l_{\Lambda=0^\circ}} \cos \Lambda \cos \Lambda_h$$

and for small angles of sideslip $\sin \beta = \beta$, $\cos \beta = 1$, and $\sin^2\beta$ is negligible, the increment in lift can be rewritten as

$$\Delta c_{l_L} = -\beta \Delta c_{l_{\Lambda=0^\circ}} \sin(\Lambda + \Lambda_h) \tag{A1}$$

The increment in primary force coefficient for a finite span wing is expressed as

$$\Delta C_{l_L} = \frac{1}{2} \Delta C_{L_L} \frac{S_f}{S_W}$$

and

$$\Delta C_{L_L} = \Delta c_{l_L} - \text{Induced lift}$$

The lift distribution resulting from sideslip is antisymmetrical with respect to the plane of symmetry; therefore, the aspect ratio that determines the magnitude of the induced angle of attack in the expression $\alpha_i = \frac{C_L}{\pi A}$ is one-half of the wing geometric aspect ratio. Since

the aspect ratio is considered perpendicular to the relative wind, the effective aspect ratio becomes $\frac{A'}{2}\frac{\cos^2(\Lambda + \beta)}{\cos^2\Lambda}$. Inasmuch as the induced angle of attack in a plane parallel to the plane of symmetry is $\alpha_i = \frac{\cos \Lambda}{\cos(\Lambda + \beta)}$, the expression for ΔC_{L_L} becomes

$$\Delta C_{L_L} \approx \Delta c_{l_L} - \frac{2\Delta C_{L_L} \cos^3\Lambda}{\pi A' \cos^3(\Lambda + \beta)} a_o \cos \Lambda$$

As explained in reference 8, the incremental primary force coefficient can be rewritten as

$$\Delta C_{l_L} = \frac{\Delta c_{l_L} \frac{S_f}{S_W}}{2} - \frac{2\Delta C_{L_L} a_o \cos^4\Lambda}{\pi A' \cos^3(\Lambda + \beta)}$$

Now the lift increment due to flap deflection for an unswept wing is given by

$$\Delta C_{L_f} = \left(a_o \alpha_\delta \delta - a_i a_o\right)\frac{S_f}{S_W}$$

The introduction of sweep changes this expression to

$$\Delta C_{L_f} = \left(a_o \alpha_\delta \delta \frac{\cos \Lambda_h}{\cos \Lambda} - \frac{\alpha_i}{\cos \Lambda} a_o\right)\cos^2\Lambda \frac{S_f}{S_W}$$

The section lift coefficient due to flap deflection and the induced angle of attack may be written as $a_o \alpha_\delta \delta = \Delta c_{l_{\Lambda=0^o}}$ and $\alpha_i = \frac{\Delta C_{L_f} \frac{S_W}{S_f}}{\pi A'}$; therefore, the expression for a swept wing becomes

$$\Delta C_{L_f} = \Delta c_{l_{\Lambda=0^o}} \frac{A' \frac{S_f}{S_W} \cos \Lambda \cos \Lambda_h}{A' + 2 \cos \Lambda} \qquad (A2)$$

With the aid of equations (A1) and (A2), ΔC_{l_L} can be reduced to

$$\Delta C_{l_L} = -\beta \frac{\Delta C_{L_f}}{2} \frac{\sin(\Lambda + \Lambda_h)}{\cos \Lambda \cos \Lambda_h} \frac{A' + 2 \cos \Lambda}{A' + 4 \cos \Lambda}$$

The total of the symmetrical and unsymmetrical values of the primary force coefficient on the left semispan is

$$C_{l_L} = \frac{\Delta C_{L_f}}{2} \left[1 - \beta \frac{\sin(\Lambda + \Lambda_h)}{\cos \Lambda \cos \Lambda_h} \frac{A' + 2 \cos \Lambda}{A' + 4 \cos \Lambda} \right] \tag{A4}$$

and by similar analysis for the right semispan

$$C_{l_R} = \frac{\Delta C_{L_f}}{2} \left[1 + \beta \frac{\sin(\Lambda + \Lambda_h)}{\cos \Lambda \cos \Lambda_h} \frac{A' + 2 \cos \Lambda}{A' + 4 \cos \Lambda} \right] \tag{A5}$$

Continuing in a manner parallel with that of reference 8 permits the primary force coefficient C_{2_L} to be expressed as

$$C_{2_L} = \frac{\left(2C_{l_L}\right)^2 \frac{S_W}{S_f}}{\pi A'} \frac{\cos^2 \Lambda}{\cos^3(\Lambda + \beta)} \tag{A6}$$

and

$$C_{2_R} = \frac{\left(2C_{l_R}\right)^2 \frac{S_W}{S_f}}{\pi A'} \frac{\cos^2 \Lambda}{\cos^3(\Lambda - \beta)} \tag{A7}$$

Since the profile drag acts parallel to the air stream, the sweep of the flap hinge line does not enter the consideration. It can be shown, therefore, that

$$\Delta C_{D_{o_L}} = \frac{\Delta C_{D_o}}{2} \frac{\cos^2(\Lambda + \beta)}{\cos^2 \Lambda} \tag{A8}$$

and

$$\Delta C_{D_{o_R}} = \frac{\Delta C_{D_o}}{2} \frac{\cos^2(\Lambda - \beta)}{\cos^2 \Lambda} \tag{A9}$$

Rolling moment.- The increment in rolling-moment coefficient due to flap deflection in sideslip can be expressed as

$$\Delta C_l = \left(C_{l_L} - C_{l_R}\right) \frac{y_{L_f}}{b} \tag{A10}$$

Equations (A4) and (A5) can be combined with equation (A10) to obtain

$$\Delta C_{l_\beta} = - \frac{\Delta C_{L_f}}{2} \frac{A' + 2 \cos \Lambda}{A' + 4 \cos \Lambda} \left(\tan \Lambda + \tan \Lambda_h\right) \frac{y_{L_f}}{b/2} \tag{A11}$$

Lateral force.- The theory indicates that the increment in lateral-force coefficient due to flap deflection in sideslip should be

$$\Delta C_Y = \left(C_{2_L} - C_{2_R}\right) \sin \Lambda - \left(\Delta C_{D_{o_L}} + \Delta C_{D_{o_R}}\right) \sin \beta \tag{A12}$$

Substituting equations (A4) to (A9) into equation (A12) gives the following expressions for the derivative:

$$\Delta C_{Y_\beta} = \frac{2\left(\Delta C_{L_f}\right)^2 \tan \Lambda}{\pi A' \frac{S_f}{S_W}} \left[\frac{3 \tan \Lambda}{2} - \frac{A' + 2 \cos \Lambda}{A' + 4 \cos \Lambda} \left(\tan \Lambda + \tan \Lambda_h\right)\right] - \Delta C_{D_o} \tag{A13}$$

Yawing moment.- The increment in yawing-moment coefficient due to flap deflection in sideslip can be expressed as

$$\Delta C_n = -\left(C_{2_L} - C_{2_R}\right) \cos \Lambda \frac{y_{L_f}}{b} - \left(C_{2_L} - C_{2_R}\right) \sin \Lambda \frac{\bar{x} - x_{L_f}}{b} +$$

$$\left(\Delta C_{D_{o_L}} - \Delta C_{D_{o_R}}\right) \cos \beta \frac{y_{D_f}}{b} + \left(\Delta C_{D_{o_L}} + \Delta C_{D_{o_R}}\right) \sin \beta \frac{\bar{x} - x_{D_f}}{b} \tag{A14}$$

With the aid of equations (A4) to (A9), the incremental derivative becomes

$$\Delta C_{n_\beta} = \frac{2\left(\Delta C_{L_f}\right)^2}{\pi A' \frac{S_f}{S_W} \cos \Lambda}\left[\frac{A' + 2 \cos \Lambda}{A' + 4 \cos \Lambda}\left(\tan \Lambda + \tan \Lambda_h\right) - \frac{3 \tan \Lambda}{2}\right]\left(\frac{\sin \Lambda}{A} \frac{\bar{x} - x_{L_f}}{\bar{c}'} + \frac{\cos \Lambda}{2} \frac{y_{L_f}}{b/2}\right) + \Delta C_{D_o}\left(\frac{\bar{x} - x_{D_f}}{A\bar{c}'} + \tan \Lambda_h \frac{y_{D_f}}{b/2}\right) \tag{A15}$$

REFERENCES

1. Queijo, M. J., and Wolhart, Walter D.: Experimental Investigation of the Effect of Vertical-Tail Size and Length and of Fuselage Shape and Length on the Static Lateral Stability Characteristics of a Model With 45° Sweptback Wing and Tail Surfaces. NACA Rep. 1049, 1951. (Supersedes NACA TN 2168.)

2. Letko, William: Effect of Vertical-Tail Area and Length on the Yawing Stability Characteristics of a Model Having a 45° Sweptback Wing. NACA TN 2358, 1951.

3. Herriot, John G.: Blockage Corrections for Three-Dimensional-Flow Closed-Throat Wind Tunnels, With Consideration of the Effect of Compressibility. NACA Rep. 995, 1950. (Supersedes NACA RM A7B28.)

4. Lichtenstein, Jacob H.: Effect of High-Lift Devices on the Low-Speed Static Lateral and Yawing Stability Characteristics of an Untapered 45° Sweptback Wing. NACA TN 2689, 1952. (Supersedes NACA RM L8G20.)

5. Thiel, G., and Weissinger, F.: Six-Component Measurements on a Straight and a 35° Swept-Back Trapezoidal Wing With and Without Split Flap. NACA TM 1107, 1947.

6. Brewer, Jack D., and Lichtenstein, Jacob H.: Effect of Horizontal Tail on Low-Speed Static Lateral Stability Characteristics of a Model Having 45° Sweptback Wing and Tail Surfaces. NACA TN 2010, 1950.

7. Goodman, Alex, and Fisher, Lewis R.: Investigation at Low Speeds of the Effect of Aspect Ratio and Sweep on Rolling Stability Derivatives of Untapered Wings. NACA Rep. 968, 1950. (Supersedes NACA TN 1835.)

8. Toll, Thomas A., and Queijo, M. J.: Approximate Relations and Charts for Low-Speed Stability Derivatives of Swept Wings. NACA TN 1581, 1948.

TABLE I

PERTINENT GEOMETRIC CHARACTERISTICS OF MODEL

Body:	
Length, in.	40.0
Fineness ratio	6.67
Wing:	
Aspect ratio	4.0
Taper ratio	0.6
Quarter-chord sweep angle, deg	45
Dihedral angle, deg	0
Twist, deg	0
NACA airfoil section	65A008
Area, sq in.	324
Span, in.	36
Mean aerodynamic chord, in.	9.19
Slats:	
Span ratio, b_s/b	0.83
Chord ratio, c_s/c	0.10
Trailing-edge split flaps:	
Chord ratio, c_f/c	0.20
Deflection from lower surface, deg	60
Outboard end of flap at -	
$0.40\frac{y_f}{b/2}$, in.	7.20
$0.70\frac{y_f}{b/2}$, in.	12.60
$1.00\frac{y_f}{b/2}$, in.	18.00
Trailing-edge plain flaps:	
Chord ratio, c_f/c	0.20
Deflection from chord line, deg	40
Outboard end of flap at -	
$0.40\frac{y_f}{b/2}$, in.	7.20
$0.70\frac{y_f}{b/2}$, in.	12.60
$1.00\frac{y_f}{b/2}$, in.	18.00

TABLE II

ORDINATES FOR NACA 65A008 AIRFOIL

[Station and ordinates in percent airfoil chord]

Station	Ordinate
0	0
.50	.615
.75	.746
1.25	.951
2.50	1.303
5.00	1.749
7.50	2.120
10.00	2.432
15.00	2.926
20.00	3.301
25.00	3.585
30.00	3.791
35.00	3.928
40.00	3.995
45.00	3.988
50.00	3.895
55.00	3.714
60.00	3.456
65.00	3.135
70.00	2.763
75.00	2.348
80.00	1.898
85.00	1.430
90.00	.960
95.00	.489
100.00	.018
L. E. radius: 0.408	

TABLE III

BODY ORDINATES

[Station and ordinates in percent body length]

Station	Ordinate
0	0
2.5	.7
5.0	1.4
7.5	2.1
10.0	2.7
12.5	3.3
15.0	3.9
20.0	4.8
25.0	5.7
30.0	6.3
35.0	6.8
40.0	7.2
45.0	7.4
50.0	7.5
55.0	7.5
60.0	7.3
65.0	7.2
70.0	6.9
75.0	6.6
80.0	6.2
85.0	5.7
90.0	5.1
95.0	4.5
100.0	3.8

TABLE IV

ORDINATES FOR SLAT AND MAIN AIRFOIL SECTION

[Stations and ordinates in percent airfoil chord]

Slat				Main airfoil[1]	
Upper surface		Lower surface		Upper surface	
Station	Ordinate	Station	Ordinate	Station	Ordinate
0	0	0	0		
.498	.622	.498	-.622		
.747	.747	.747	-.747		
1.253	.951	1.253	-.951		
2.498	1.298	2.000	-1.173	2.000	-1.173
4.996	1.751	2.667	-.098	2.667	-.098
7.502	2.116	3.333	.338	3.333	.338
10.000	2.427	4.000	.658	4.000	.658
15.004	2.933	4.667	.924	4.667	.924
		5.333	1.173	5.333	1.173
		6.222	1.449	6.222	1.449
		7.111	1.689	7.111	1.689
		8.000	1.902	8.000	1.902
		8.889	2.116	8.889	2.116
		9.778	2.311	9.778	2.311
		10.000	2.338	10.000	2.338
		15.004	2.933	10.667	2.480
				11.556	2.613
				15.004	2.933

[1]Behind the 15-percent station, the upper surface of the airfoil is the same as the basic NACA 65A008 airfoil.

Behind the 2-percent station, the lower surface of the main airfoil is the same as the basic NACA 65A008 airfoil.

TABLE V

CONFIGURATIONS INVESTIGATED AND INDEX TO THE FIGURES HAVING DATA ON THESE CONFIGURATIONS

Slats retracted		Slats extended	
Configuration[1]	Figure	Configuration[1]	Figure
WB	4,5,8(a),8(b)	WB + S	6,7,8(c),8(d)
WB + F_1	4,8(a),10	WB + S + F_1	6,8(c),10
WB + F_2	4,8(a),10	WB + S + F_2	6,8(c),10
WB + F_3	4,8(a),10	WB + S + F_3	6,8(c),10
WB + F_4	5,8(b),10	WB + S + F_4	7,8(d),10
WB + F_5	5,8(b),10	WB + S + F_5	7,8(d),10
WB + F_6	5,8(b),10	WB + S + F_6	7,8(d),10

[1] WB wing-body configuration
S slats extended
F flap; subscripts 1, 2, and 3 refer to plain flap of $0.4\frac{b}{2}$, $0.7\frac{b}{2}$, and $1.0\frac{b}{2}$, and subscripts 4, 5, and 6 refer to split flap of $0.4\frac{b}{2}$, $0.7\frac{b}{2}$, and $1.0\frac{b}{2}$.

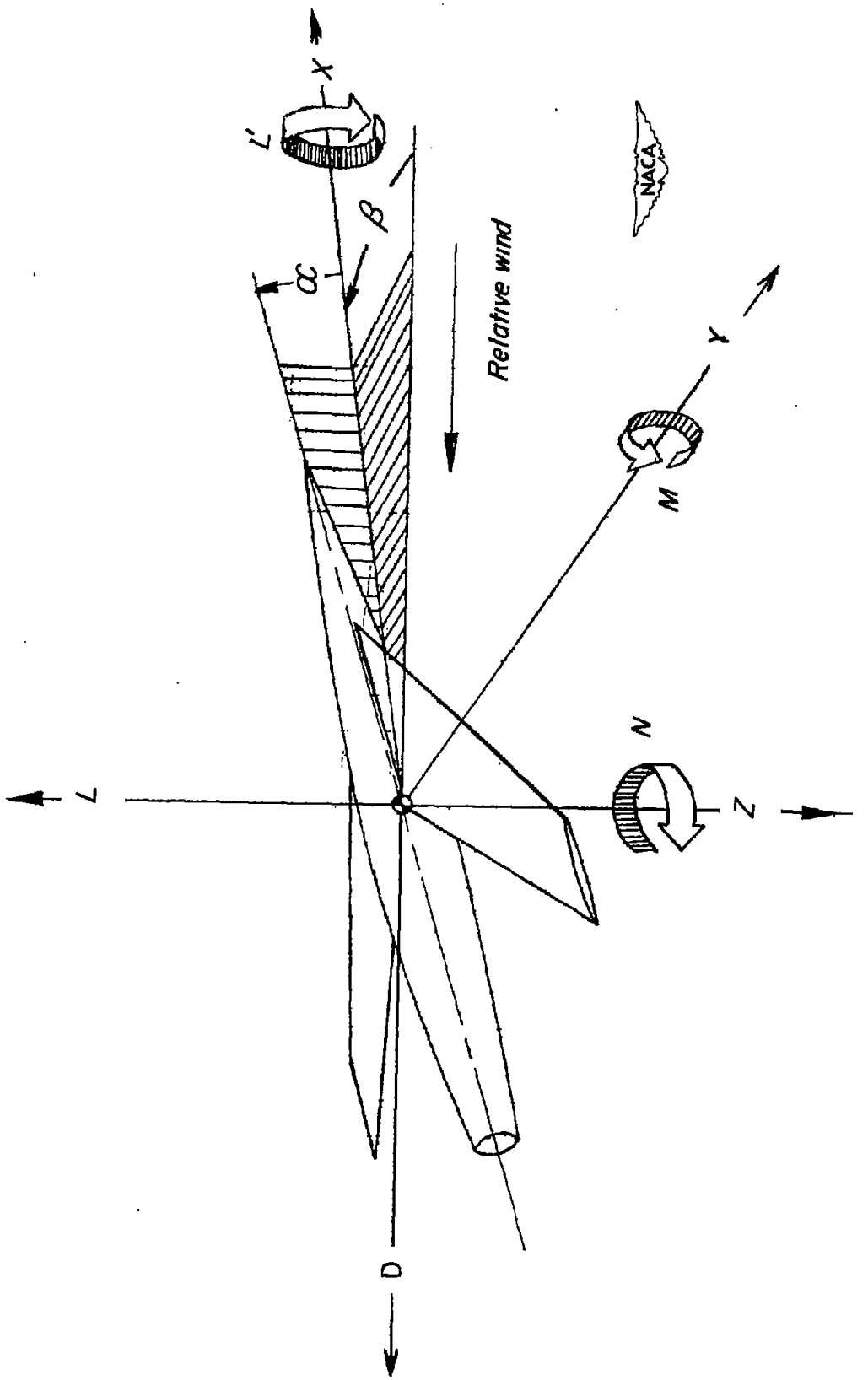

Figure 1.- System of axes used. Arrows indicate positive direction of angles, forces, and moments.

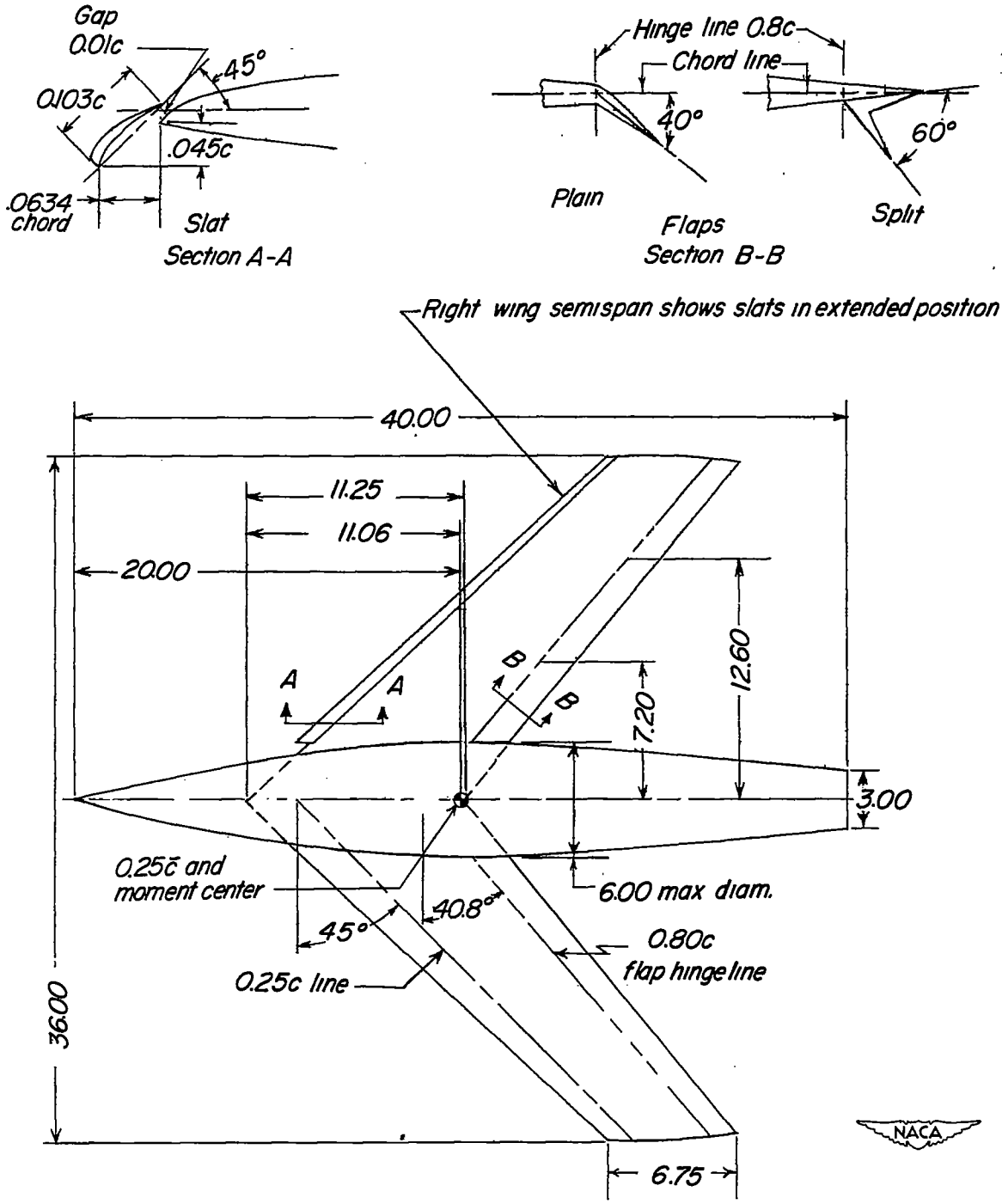

Figure 2.- Dimensions of the model. Wing has aspect ratio of 4, taper ratio of 0.6, and was mounted along the body center line. All dimensions are in inches.

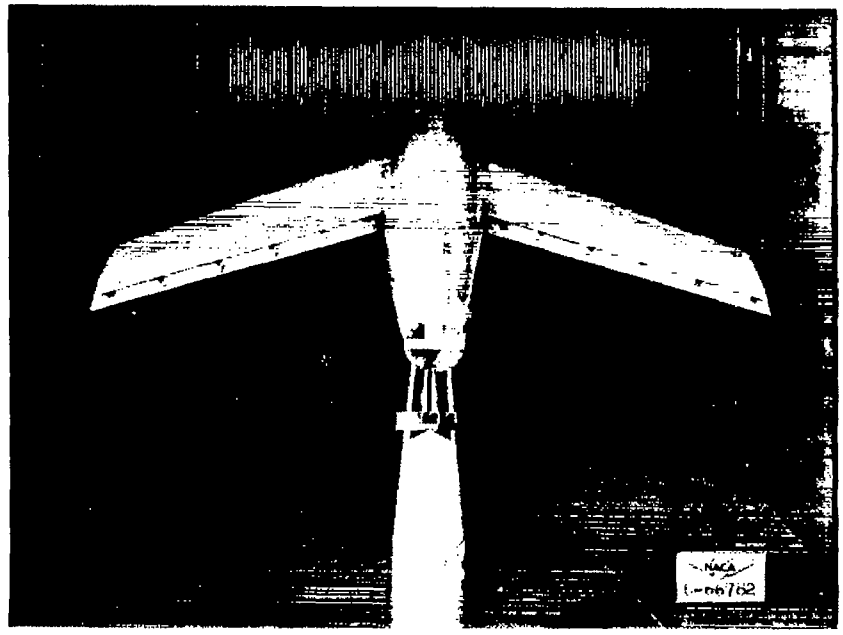

(a) Wing-body configuration with full-span split flap.

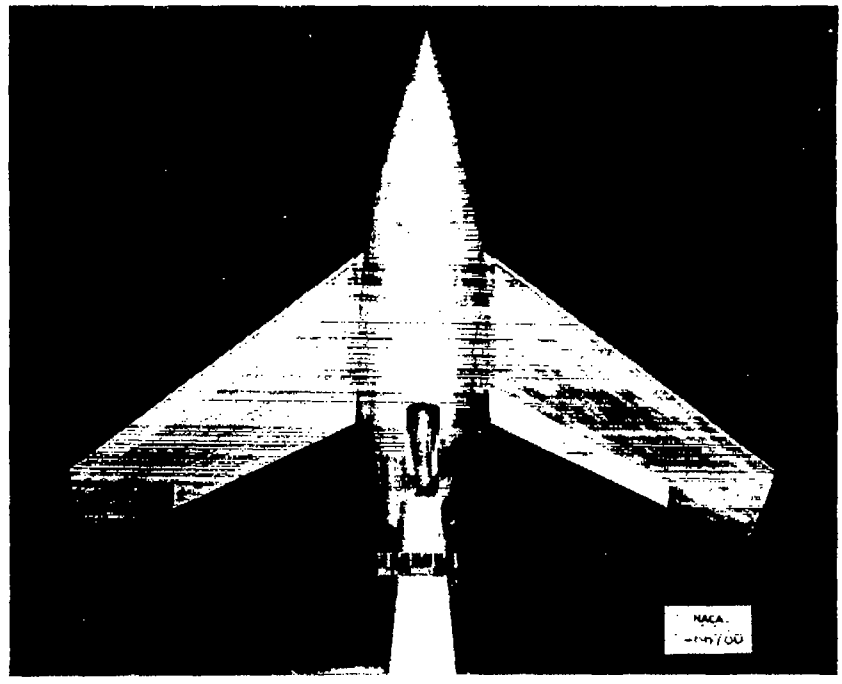

(b) Wing-body configuration with slats and $0.7\frac{b}{2}$ plain flaps.

Figure 3.- Model as mounted in the Langley stability tunnel for testing.

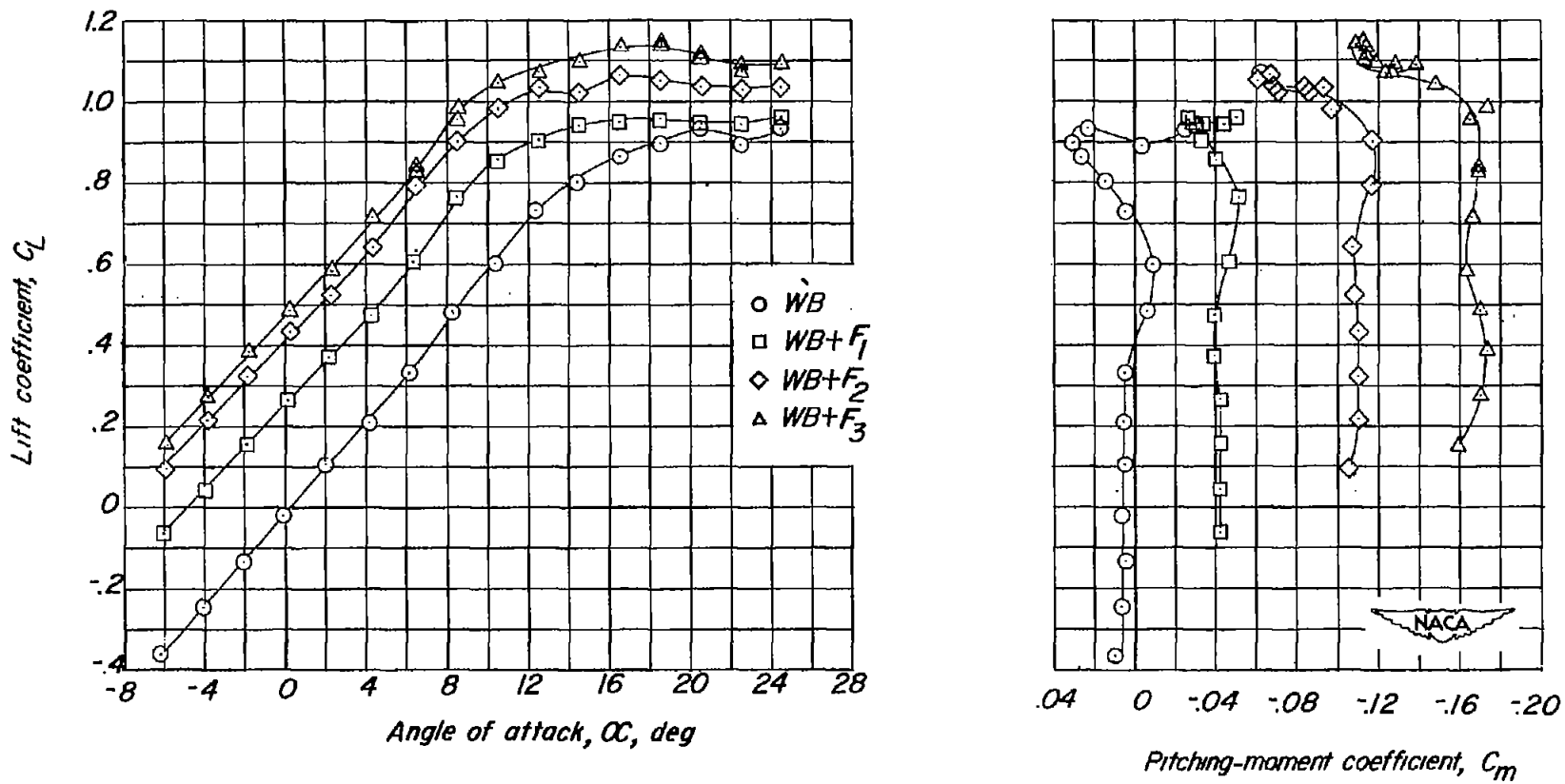

Figure 4.- Variation of angle of attack, pitching-moment coefficient, and drag coefficient with lift coefficient for the wing-body configuration with plain flaps of various span deflected.

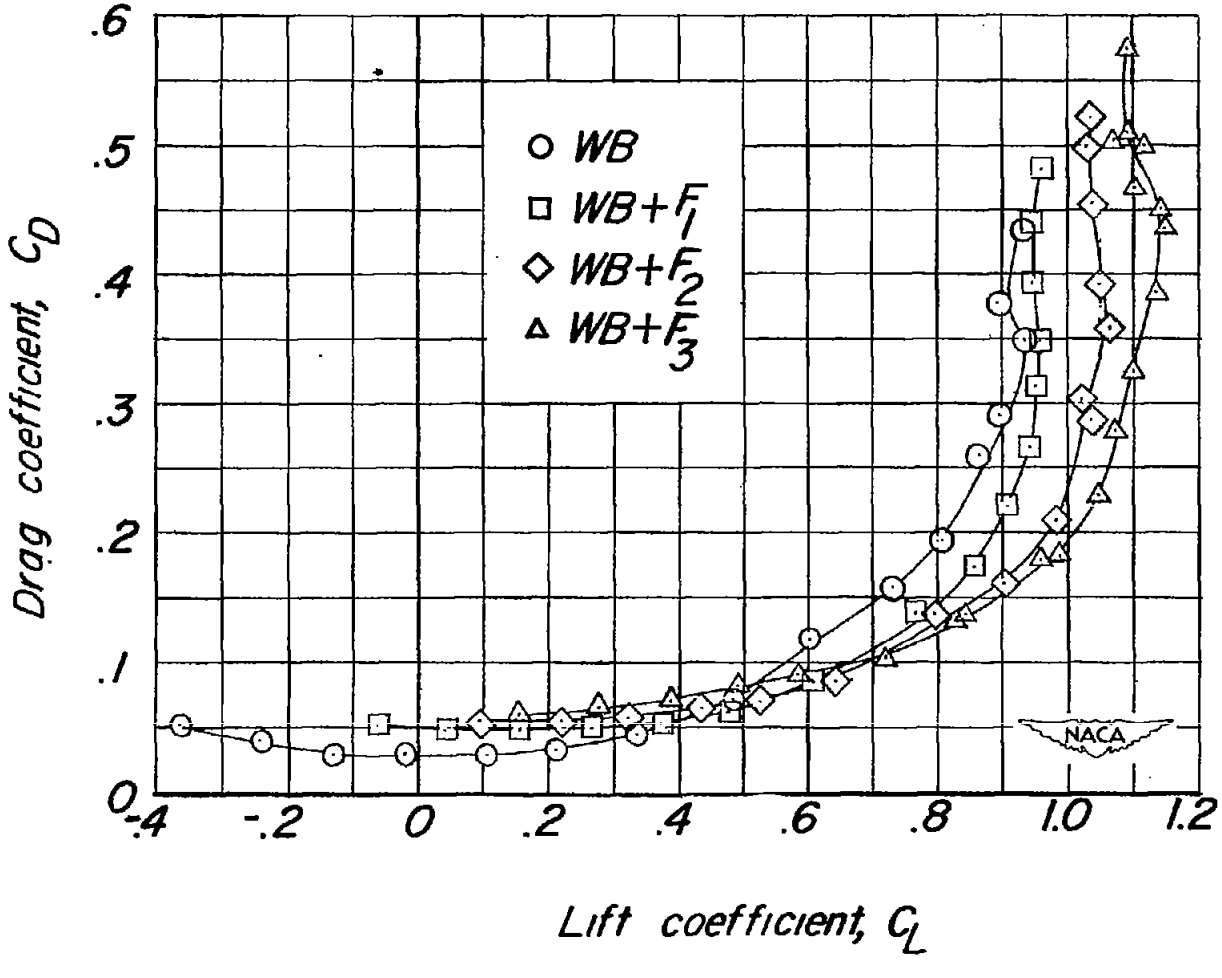

Figure 4.- Concluded.

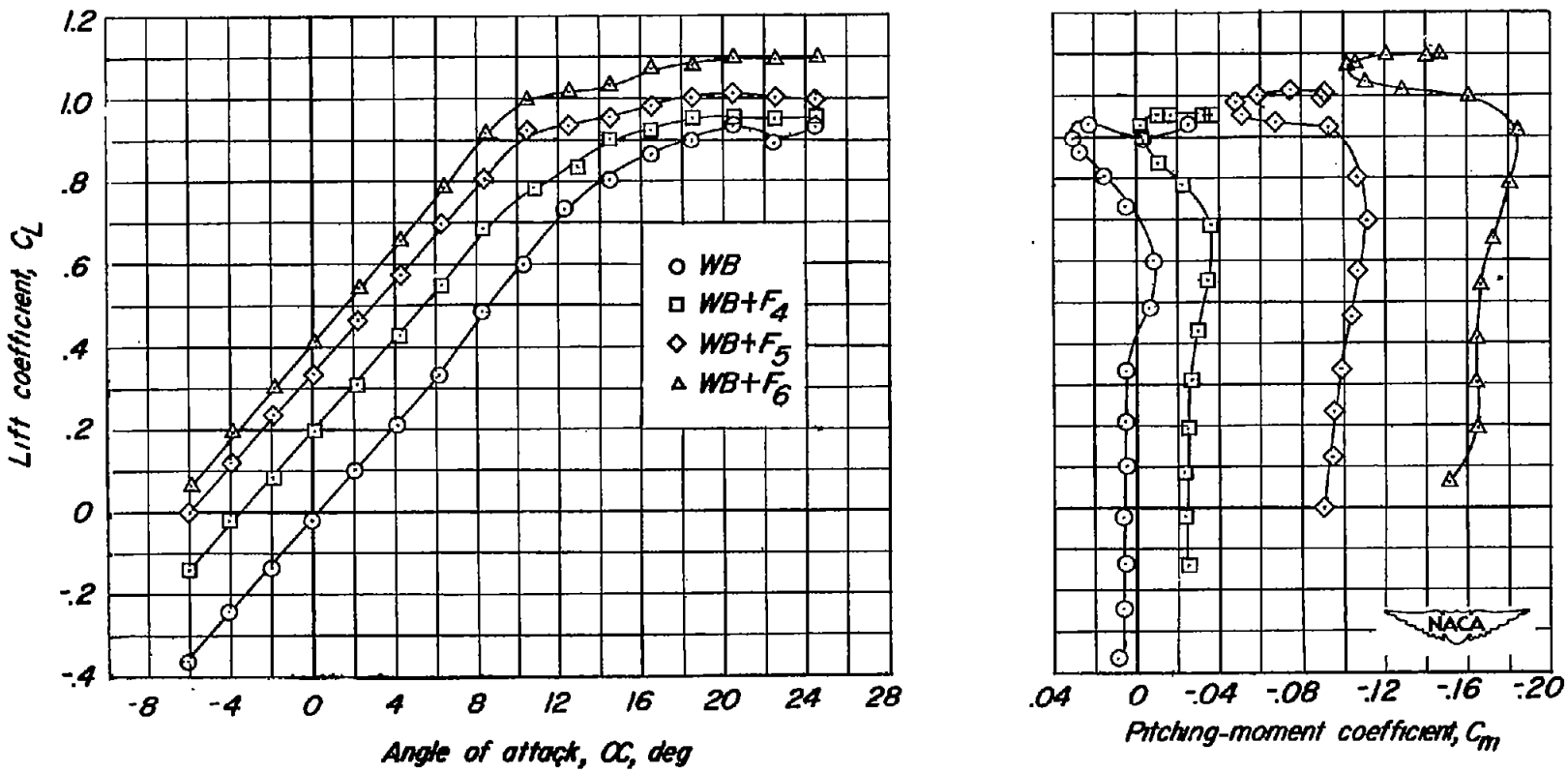

Figure 5.- Variation of angle of attack, pitching-moment coefficient, and drag coefficient with lift coefficient for the wing-body configuration with split flaps of various span deflected.

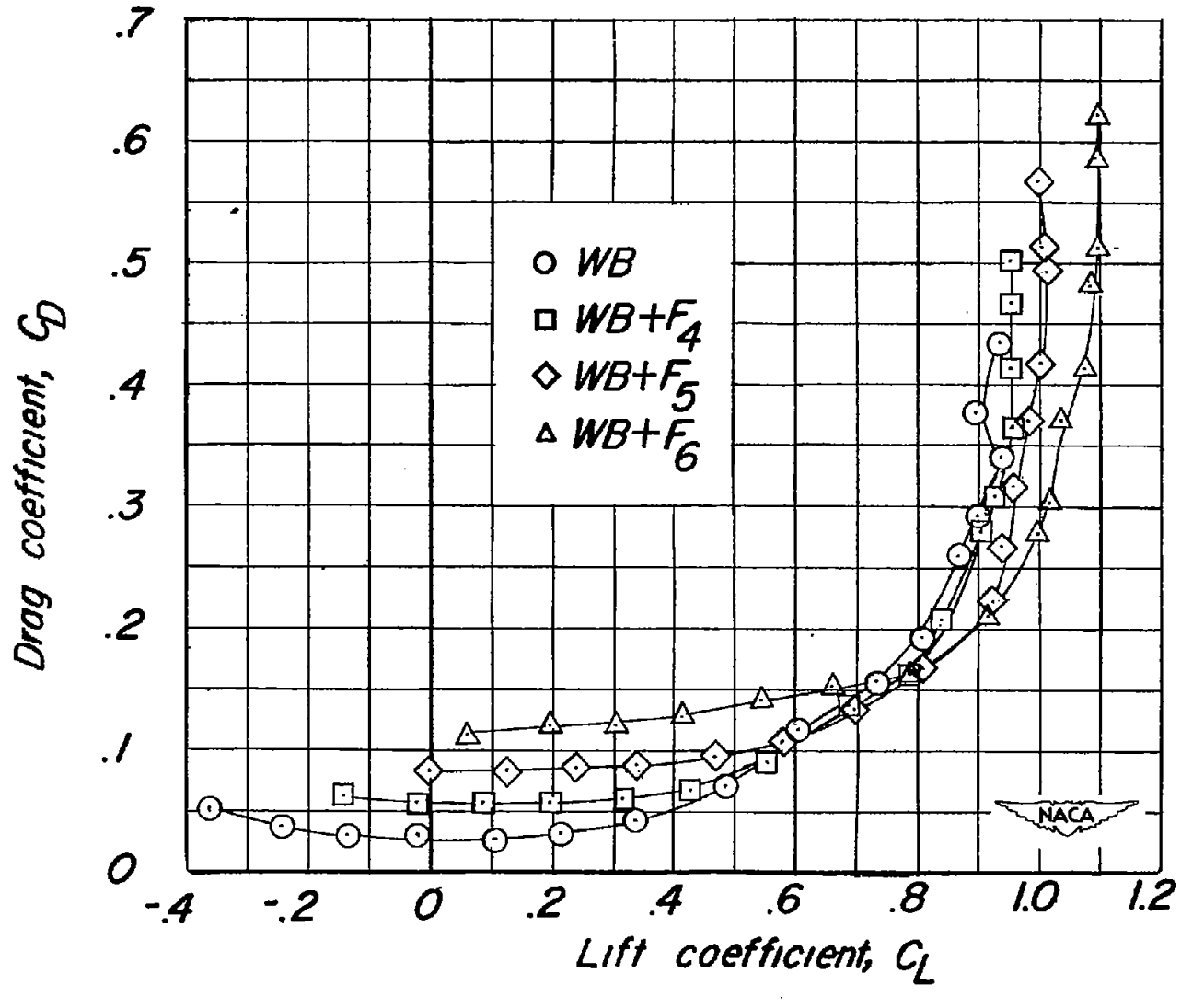

Figure 5.- Concluded.

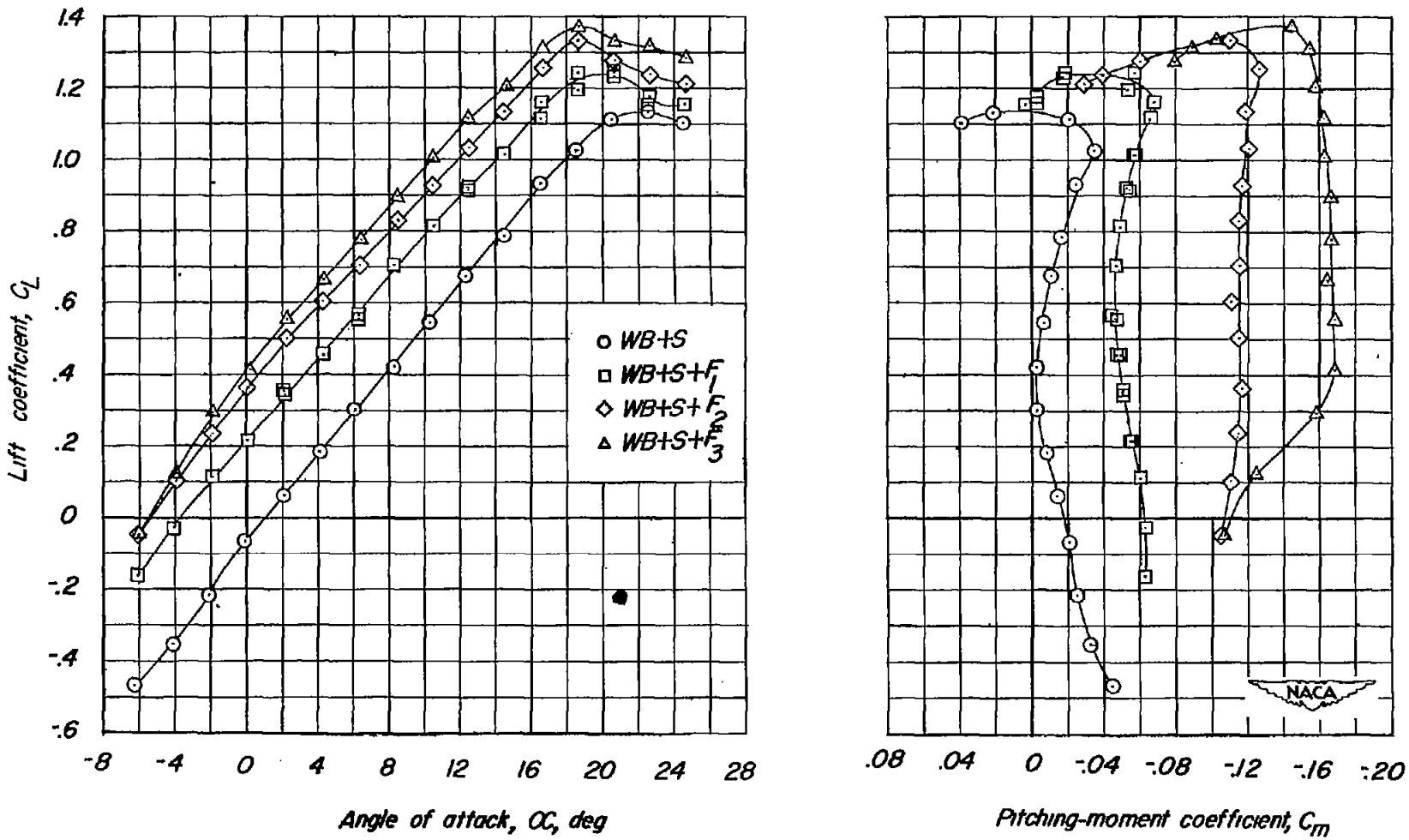

Figure 6.- Variation of angle of attack, pitching-moment coefficient, and drag coefficient with lift coefficient for the wing-body configuration with slats extended and plain flaps of various span deflected.

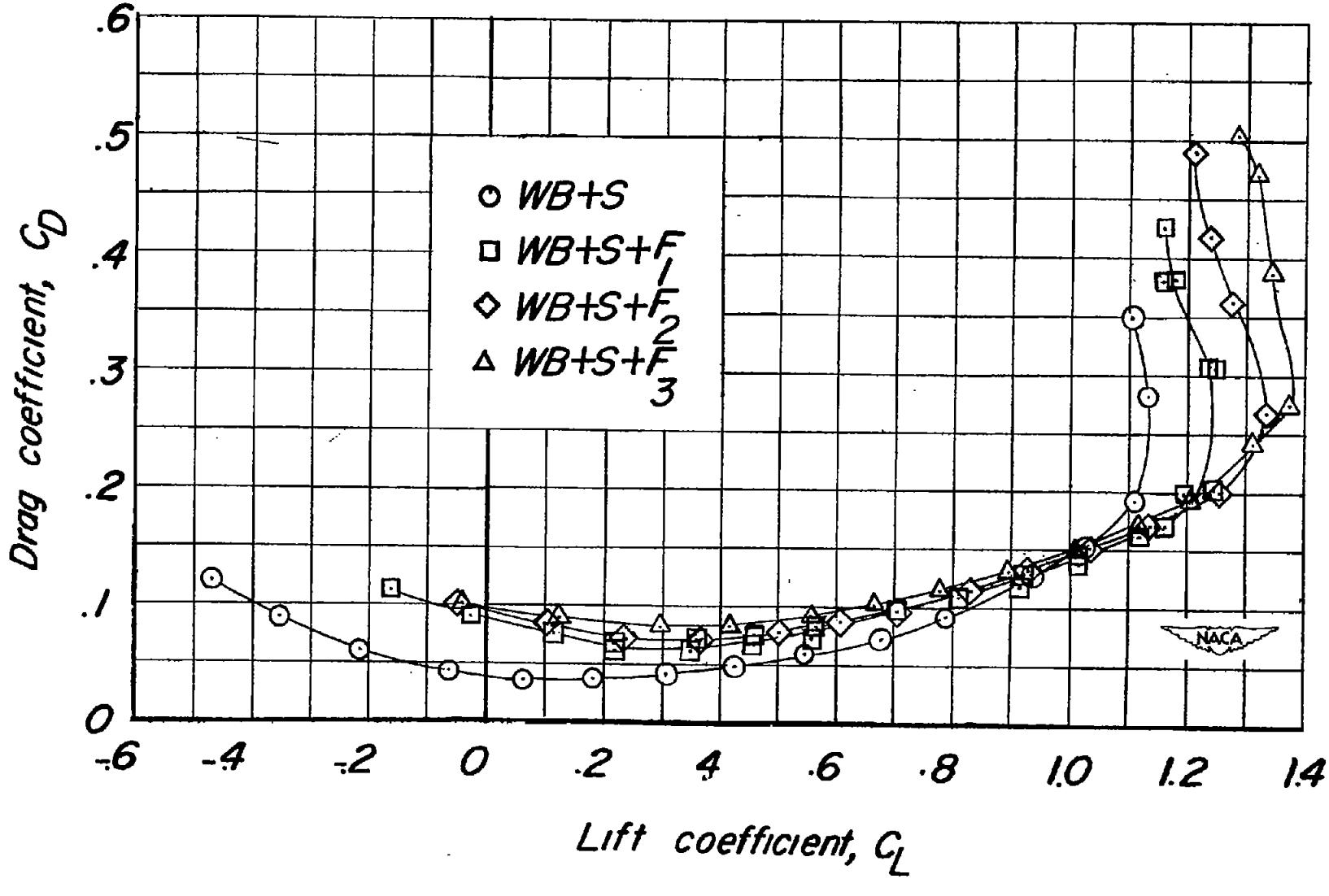

Figure 6.- Concluded.

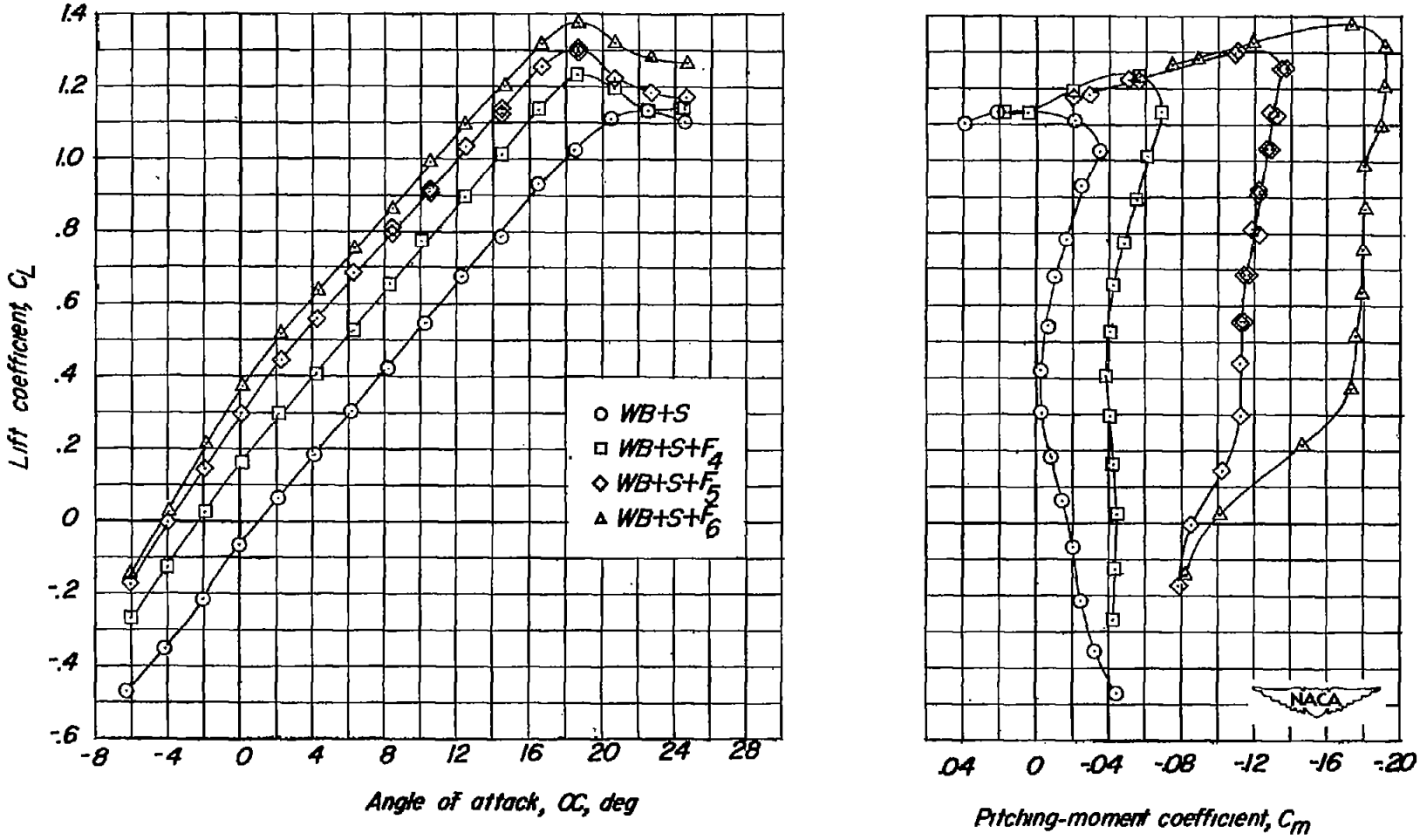

Figure 7.- Variation of angle of attack, pitching-moment coefficient, and drag coefficient with lift coefficient for the wing-body configuration with slats extended and split flaps of various span deflected.

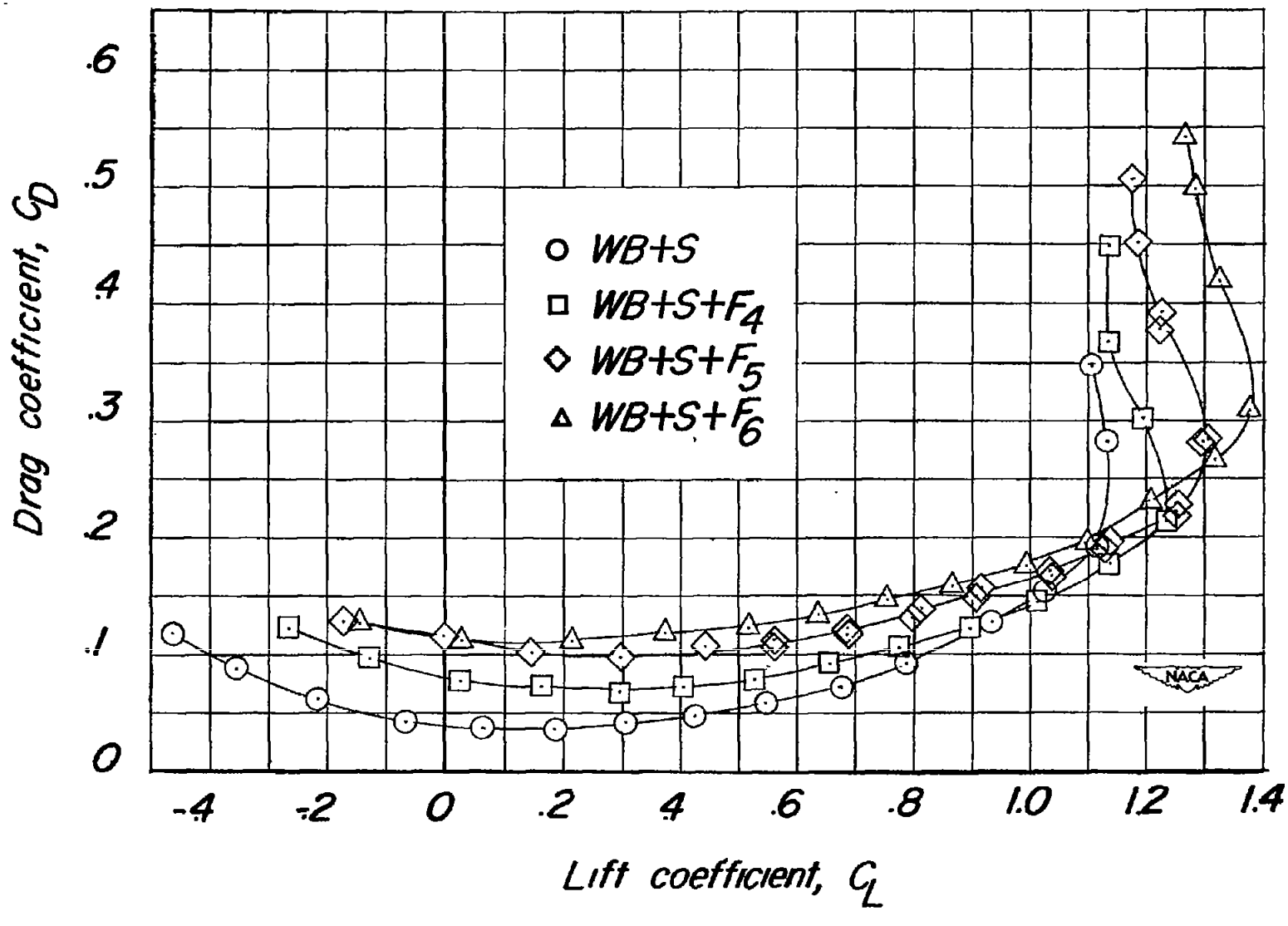

Figure 7.- Concluded.

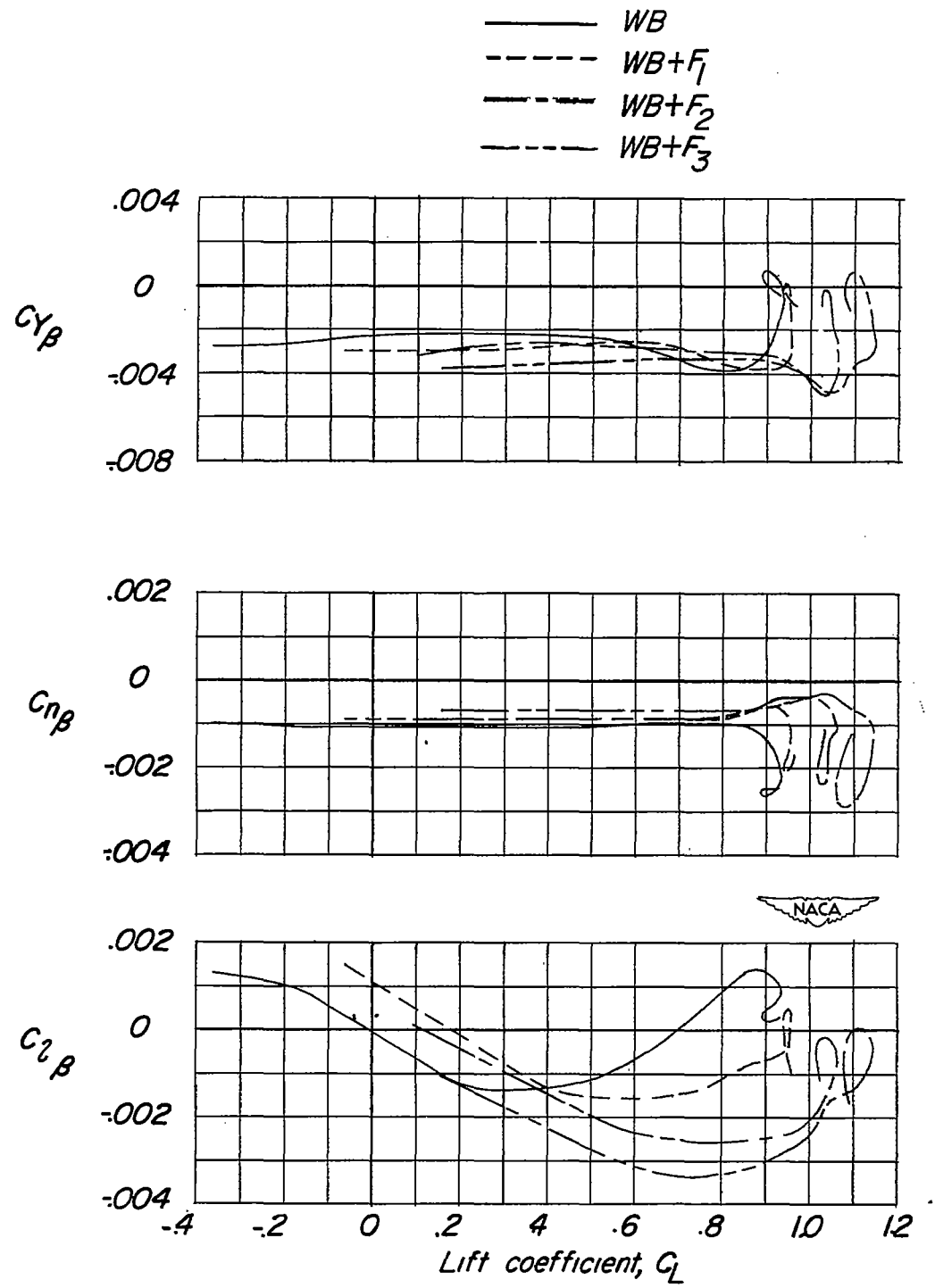

(a) Wing-body configuration with plain flaps deflected.

Figure 8.- Variation of the static-lateral-stability parameters with lift coefficient for the various configurations tested.

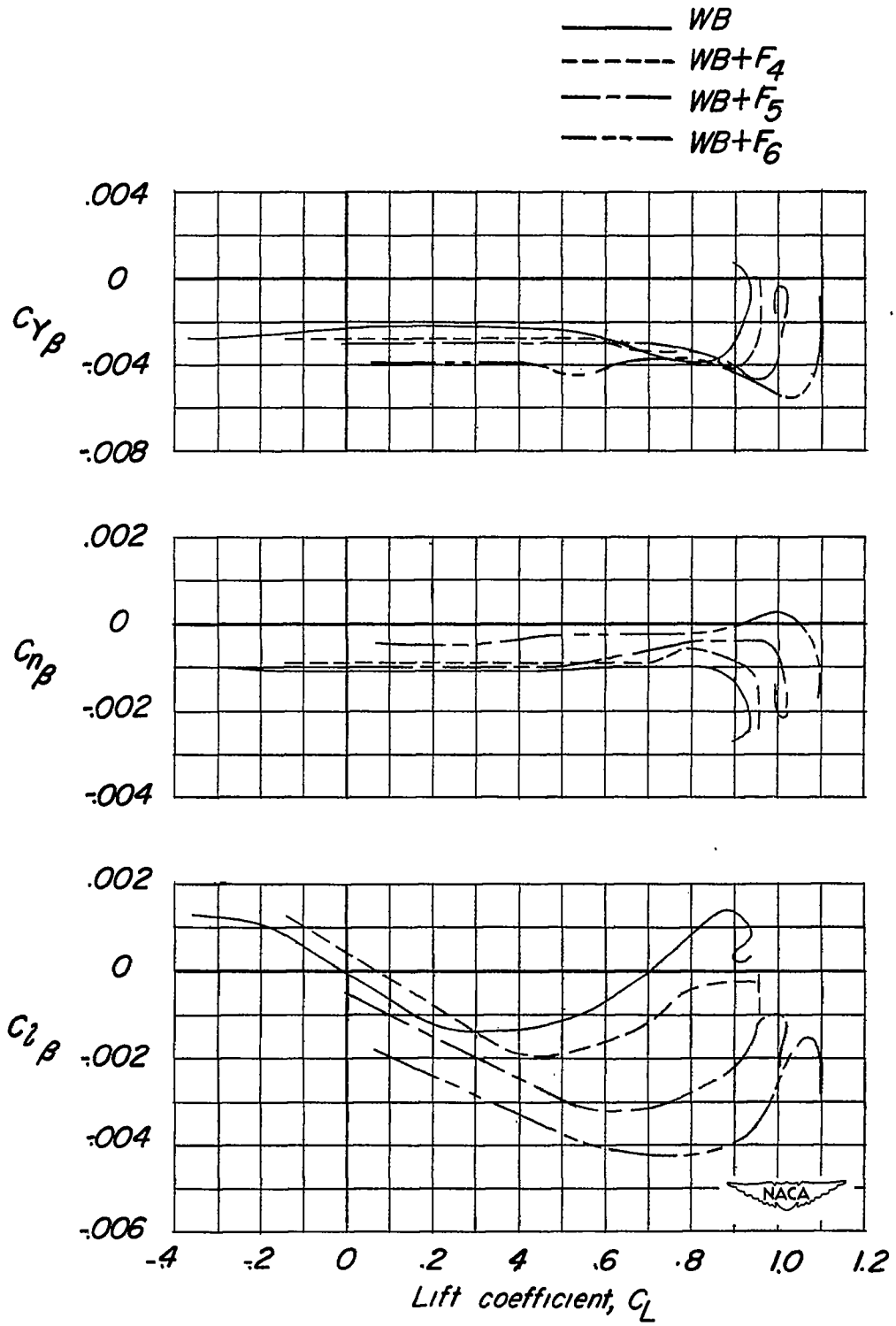

(b) Wing-body configuration with split flaps deflected.

Figure 8.- Continued.

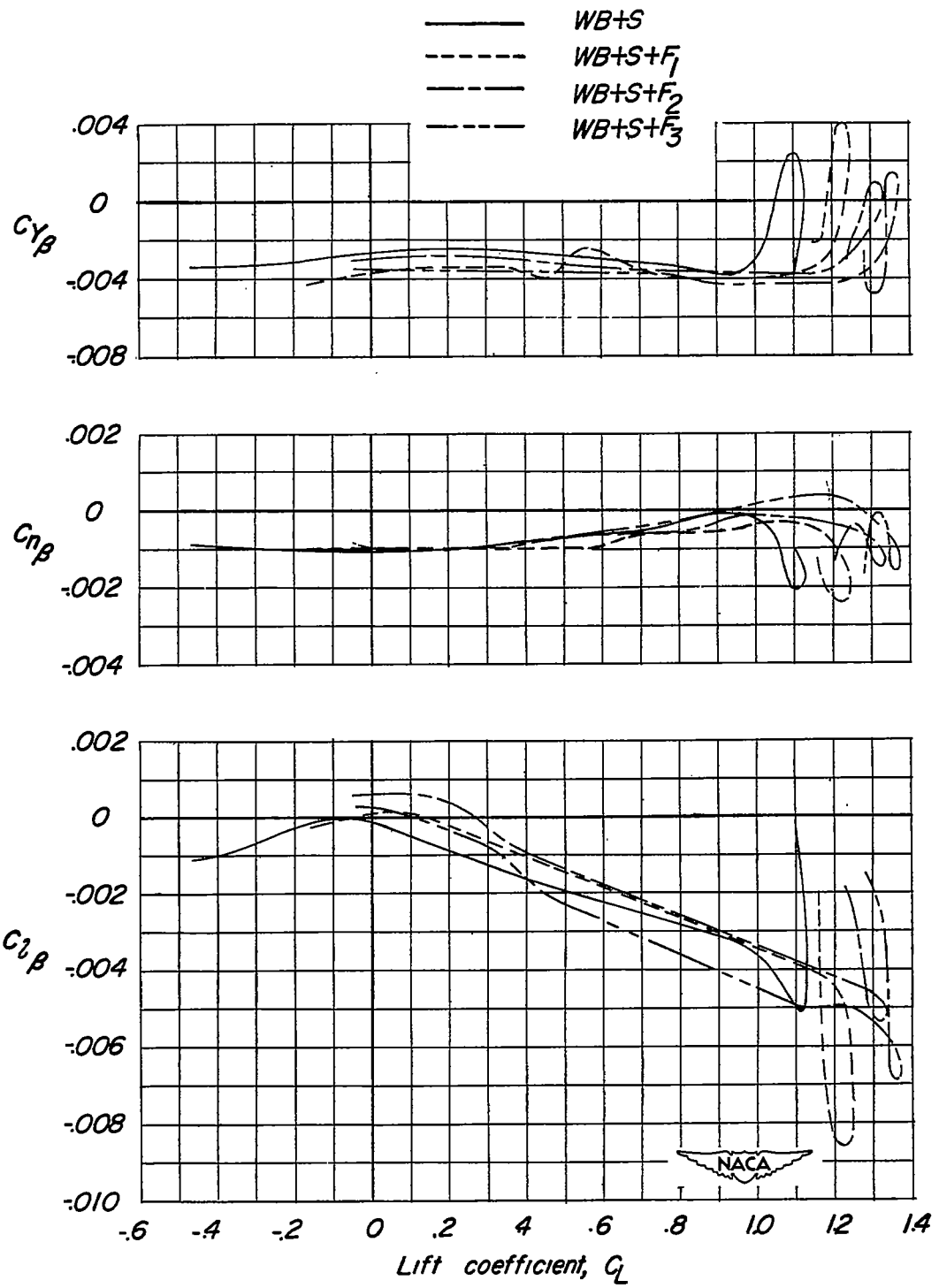

(c) Wing-body configuration with slats extended and plain flaps deflected.

Figure 8.- Continued.

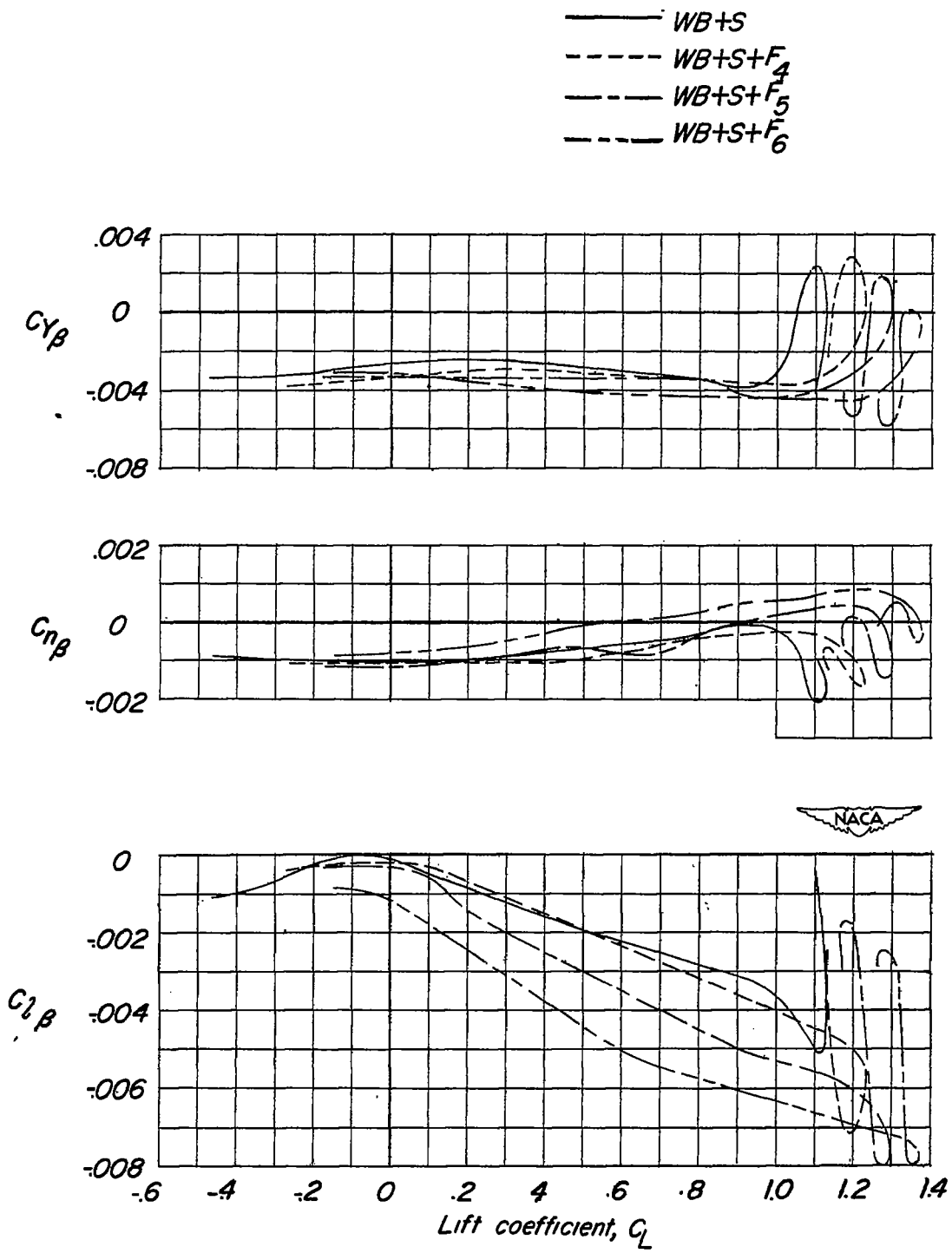

(d) Wing-body configuration with slats extended and split flaps deflected.

Figure 8.- Concluded.

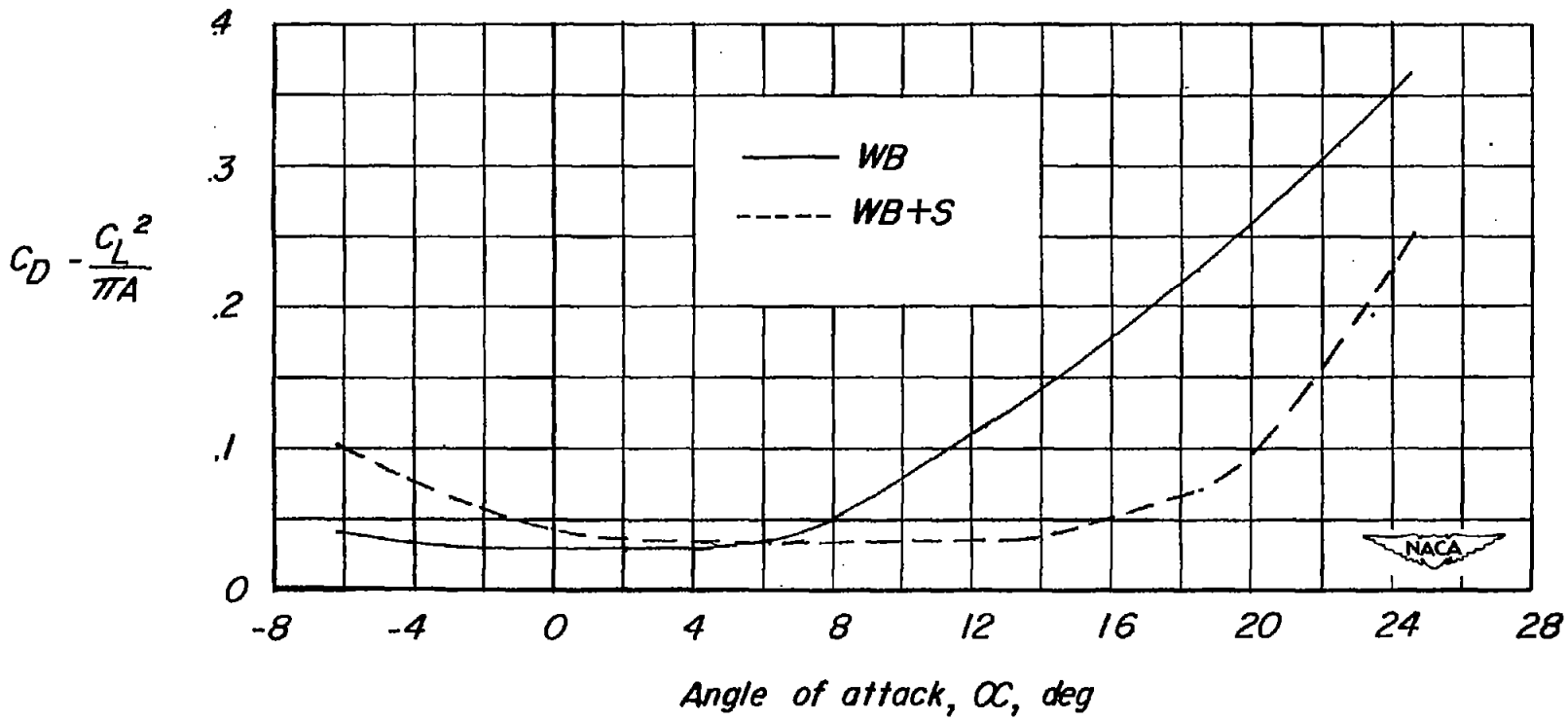

Figure 9.- Variation of $C_D - \frac{C_L^2}{\pi A}$ with angle of attack for the wing-body configuration and the wing-body configuration with slats extended.

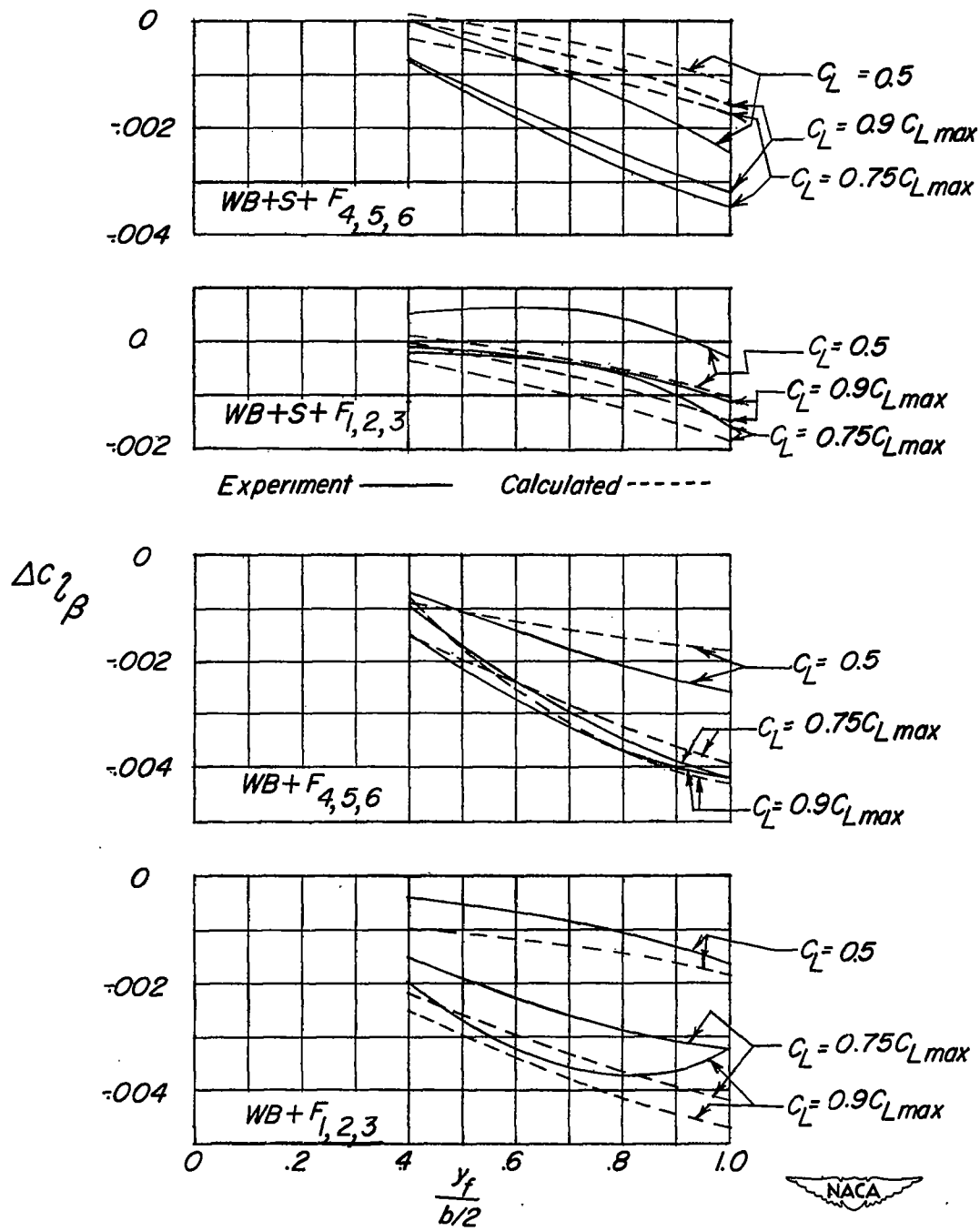

(a) ΔC_{l_β} against $\frac{y_f}{b/2}$.

Figure 10.- Comparison of experimental and calculated increments in static-lateral-stability derivatives due to deflection of trailing-edge flaps with and without leading-edge slats extended for flaps of various span. Wing-body configuration; A = 4; $\Lambda = 45^\circ$; $\lambda = 0.6$.

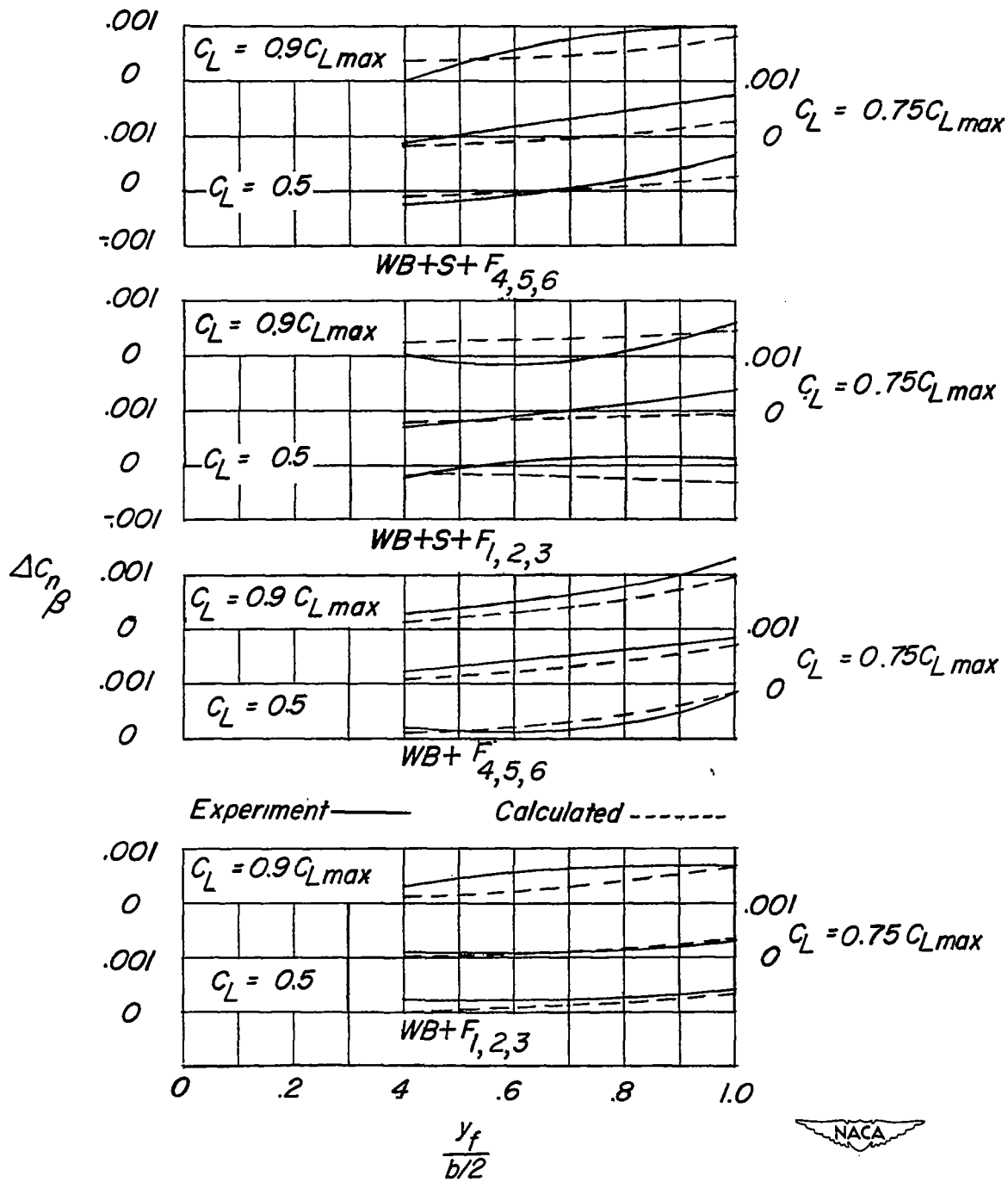

(b) ΔC_{n_β} against $\frac{y_f}{b/2}$.

Figure 10.- Continued.

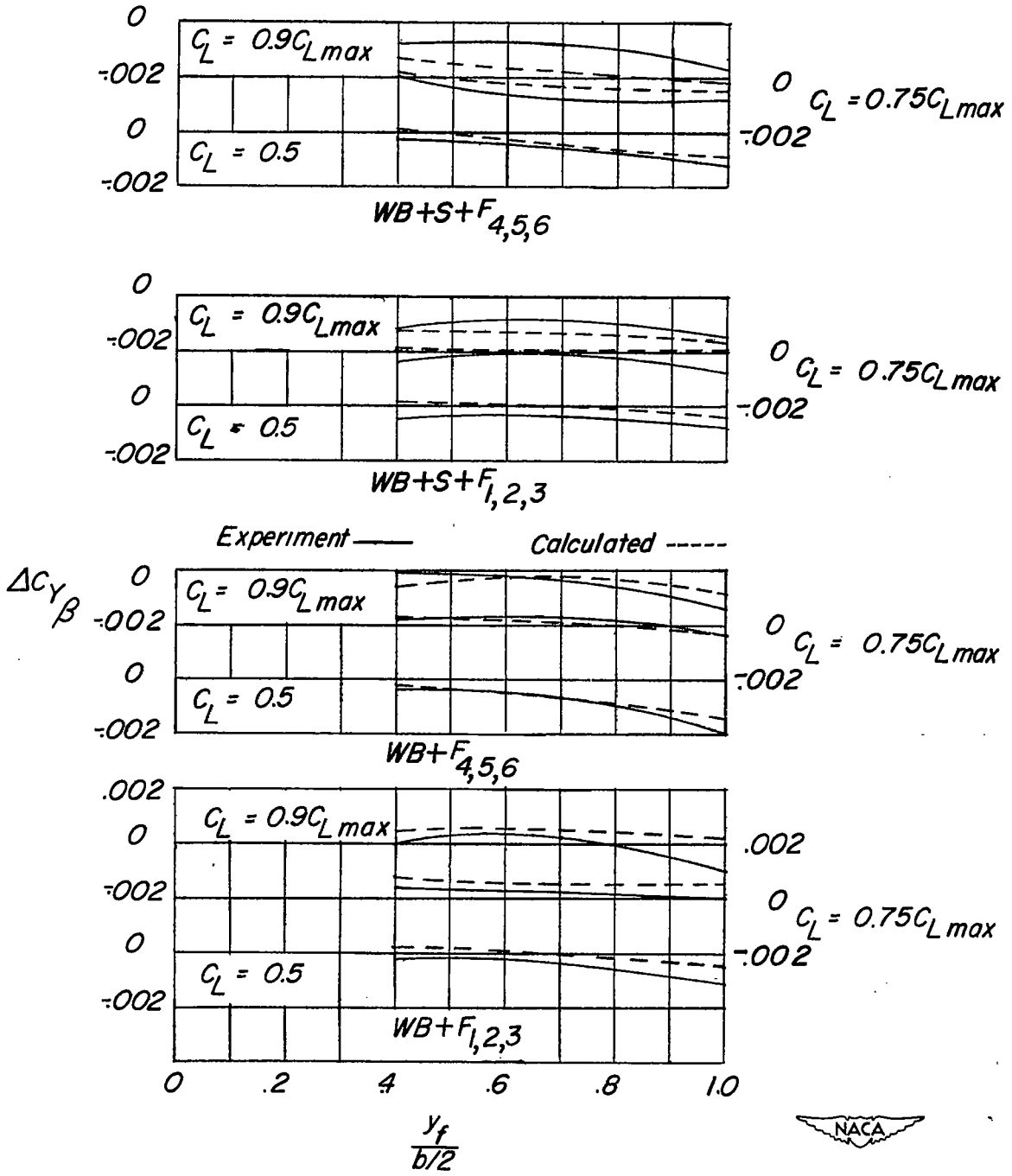

(c) ΔC_{Y_β} against $\frac{y_f}{b/2}$.

Figure 10.- Concluded.

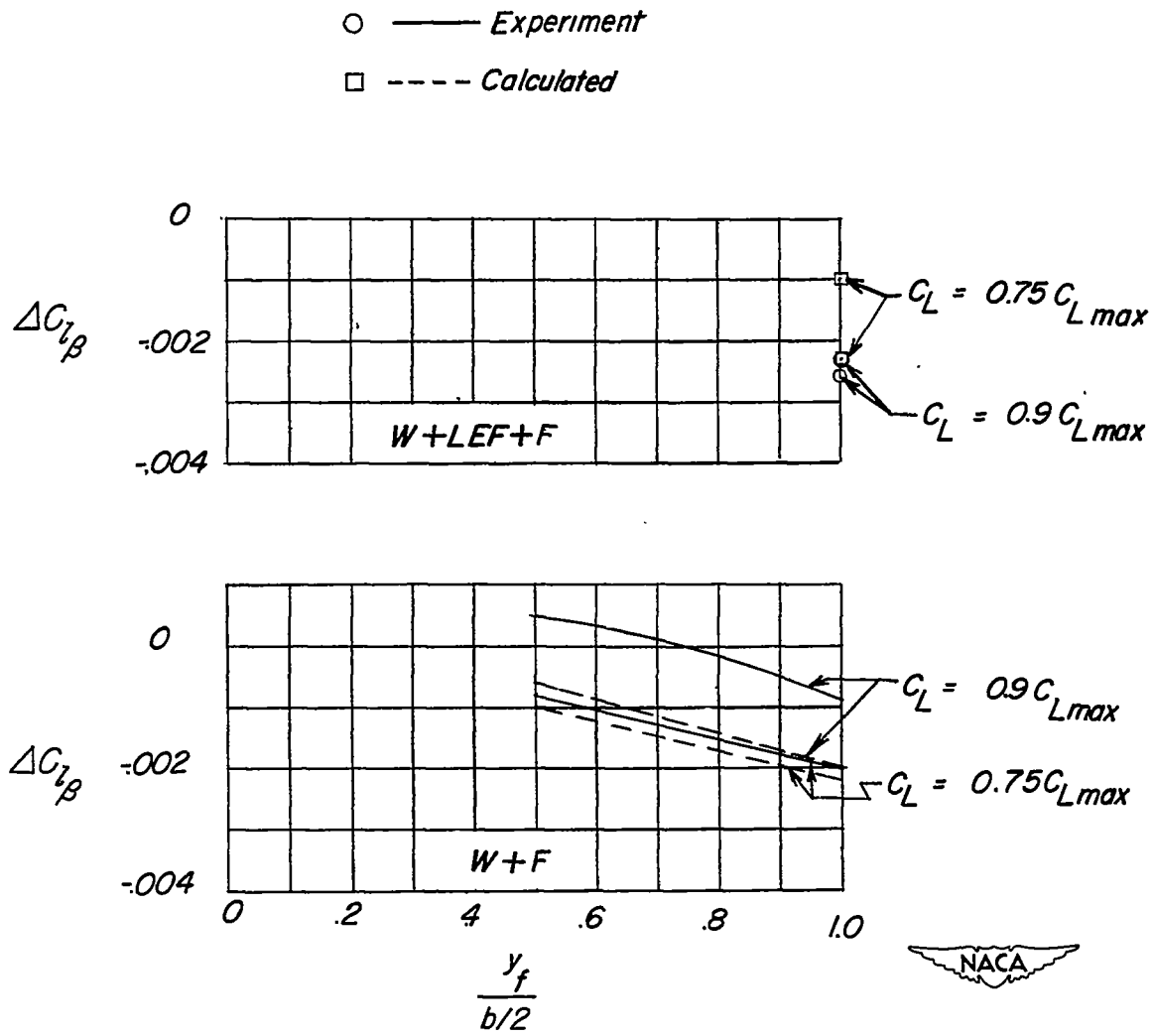

(a) ΔC_{l_β} against $\frac{y_f}{b/2}$.

Figure 11.- Comparison of experimental and calculated increments in static-lateral-stability derivatives due to deflection of trailing-edge split flaps (F) with and without leading-edge flaps (LEF) for various flap spans for the wing of reference 4. A = 2.61; $\Lambda = 45^\circ$; $\lambda = 1$.

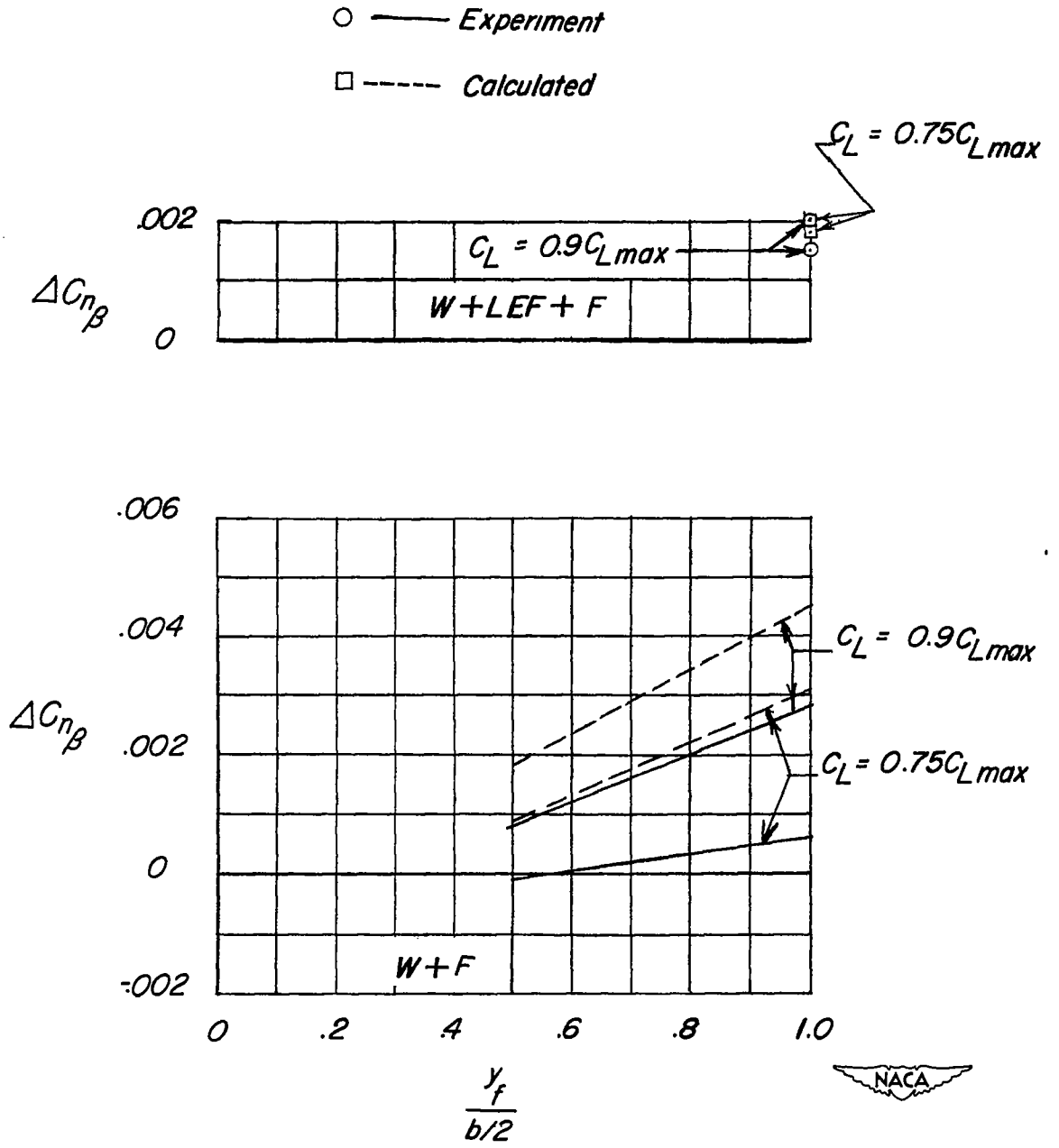

(b) ΔC_{n_β} against $\frac{y_f}{b/2}$.

Figure 11.- Continued.

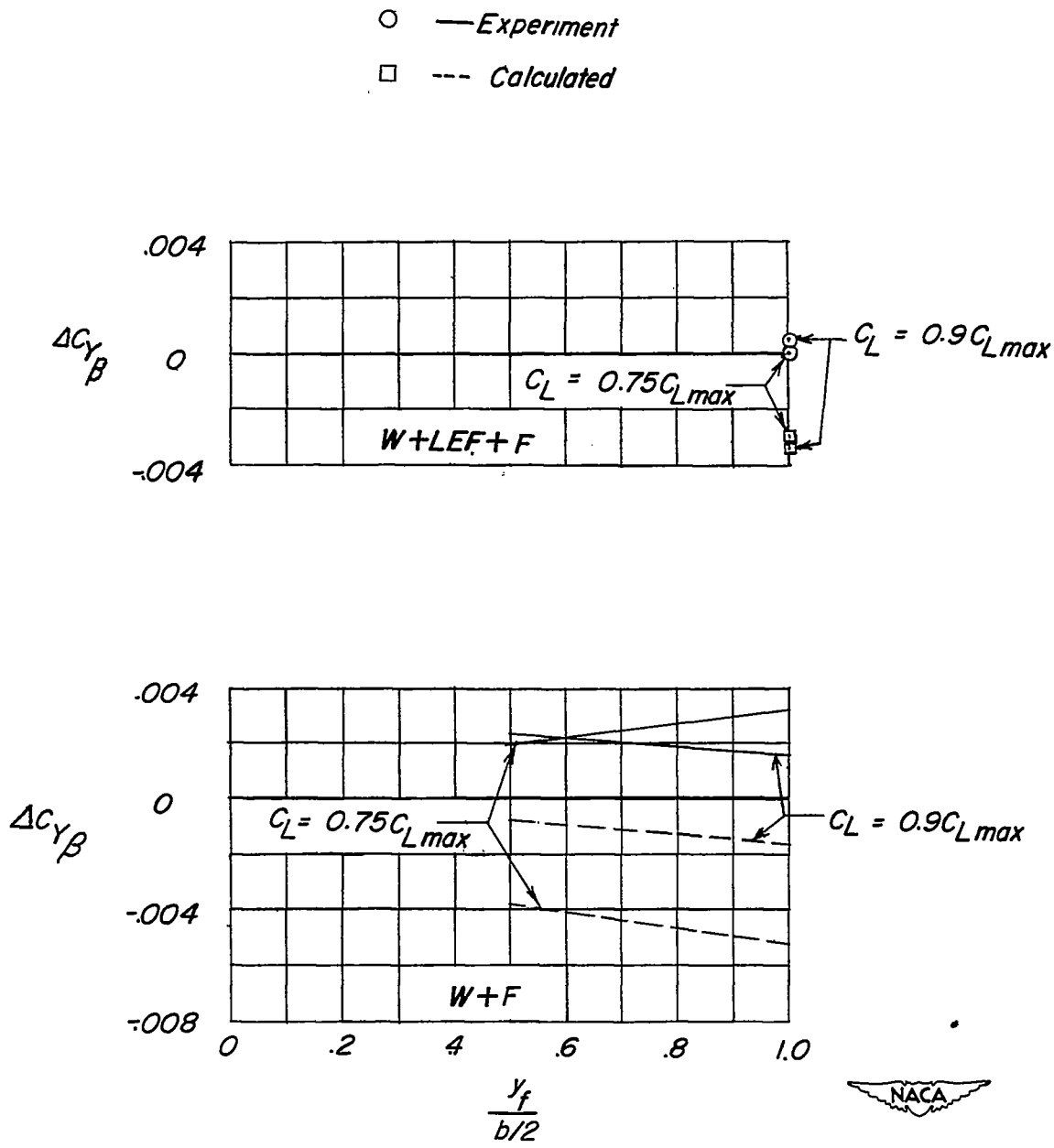

(c) ΔC_{Y_β} against $\frac{y_f}{b/2}$.

Figure 11.- Concluded.

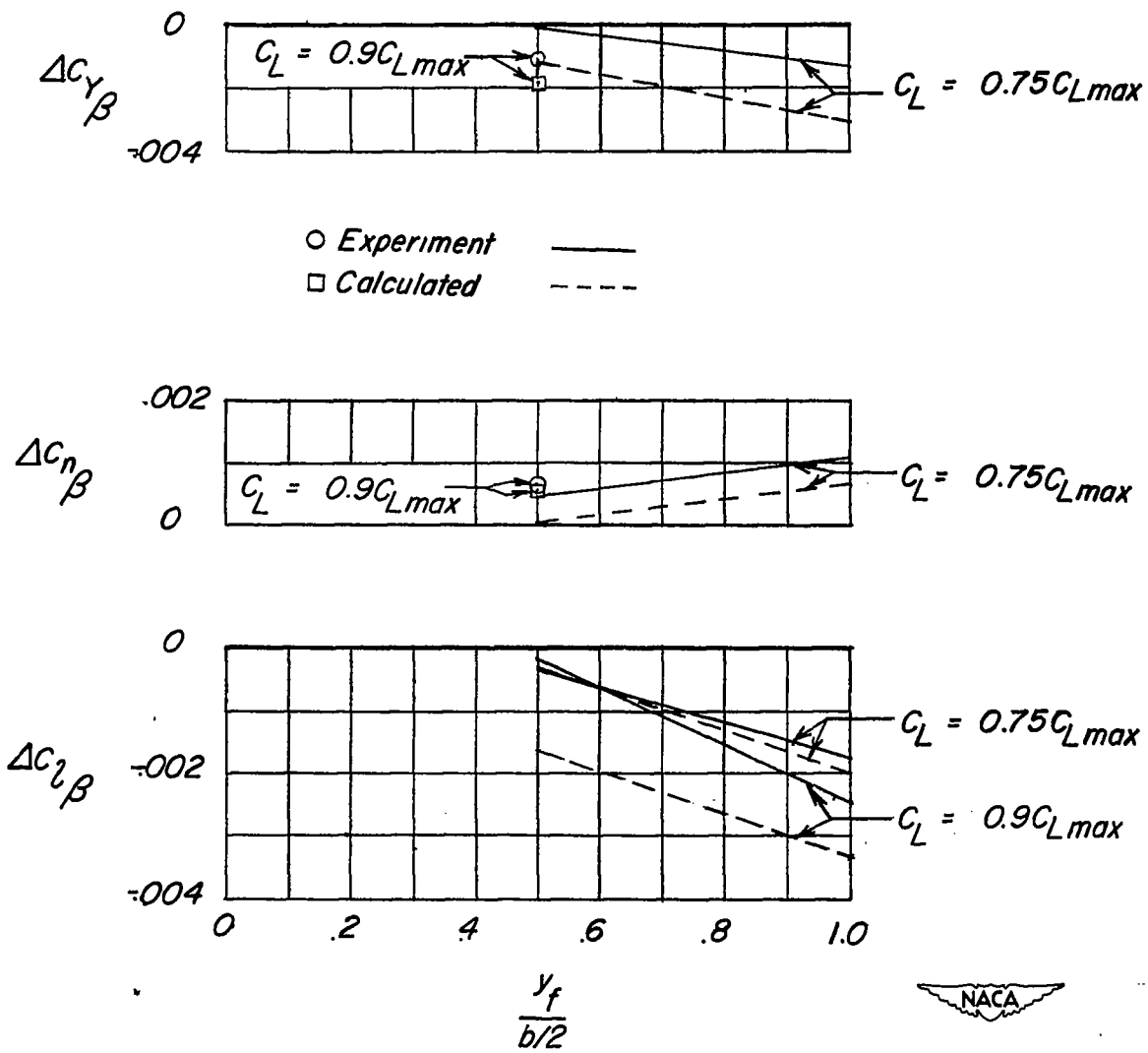

Figure 12.- Comparison of experimental and calculated increments in static-lateral-stability derivatives due to deflection of trailing-edge split flaps of various spans for the wing of reference 5. $A = 5$; $\Lambda = 35^\circ$; $\lambda = 0.5$.

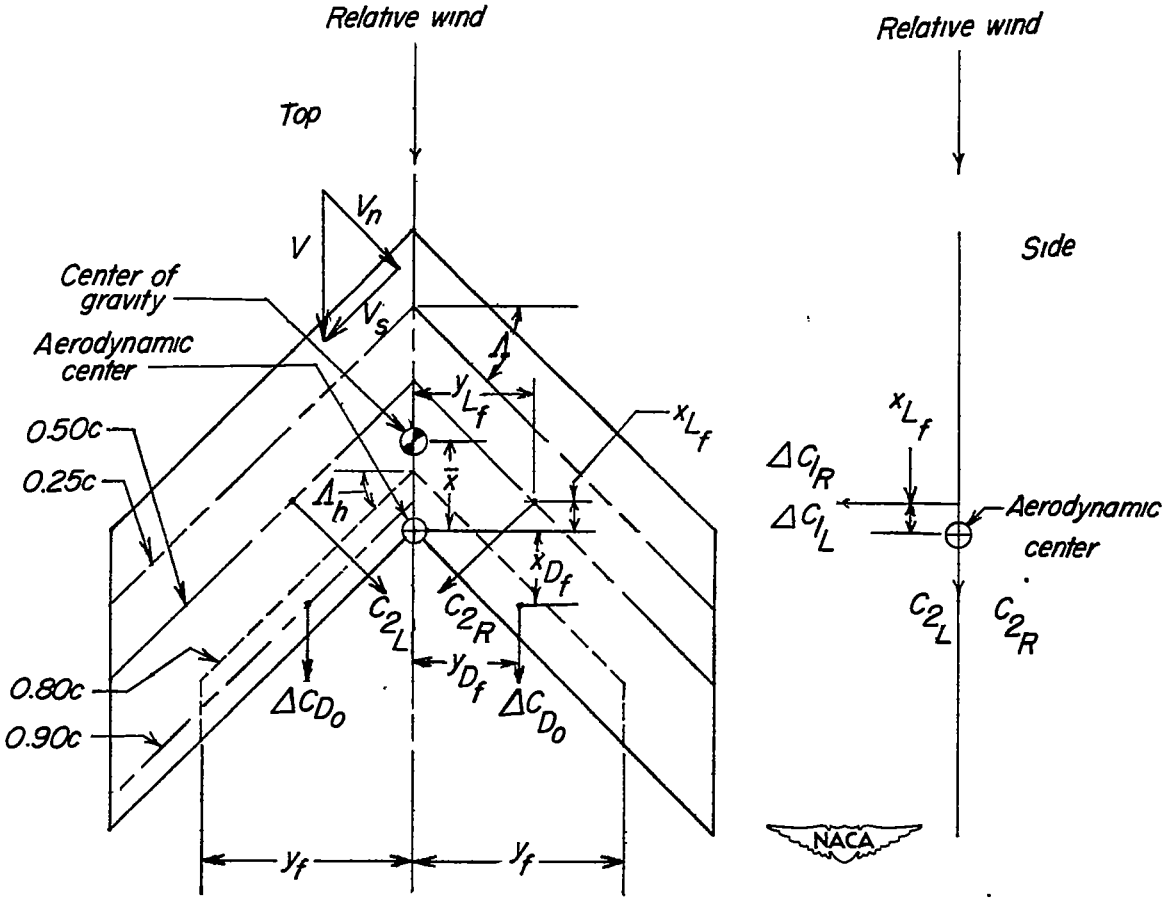

Figure 13.- Location and orientation of forces due to flap deflection considered in this analysis.

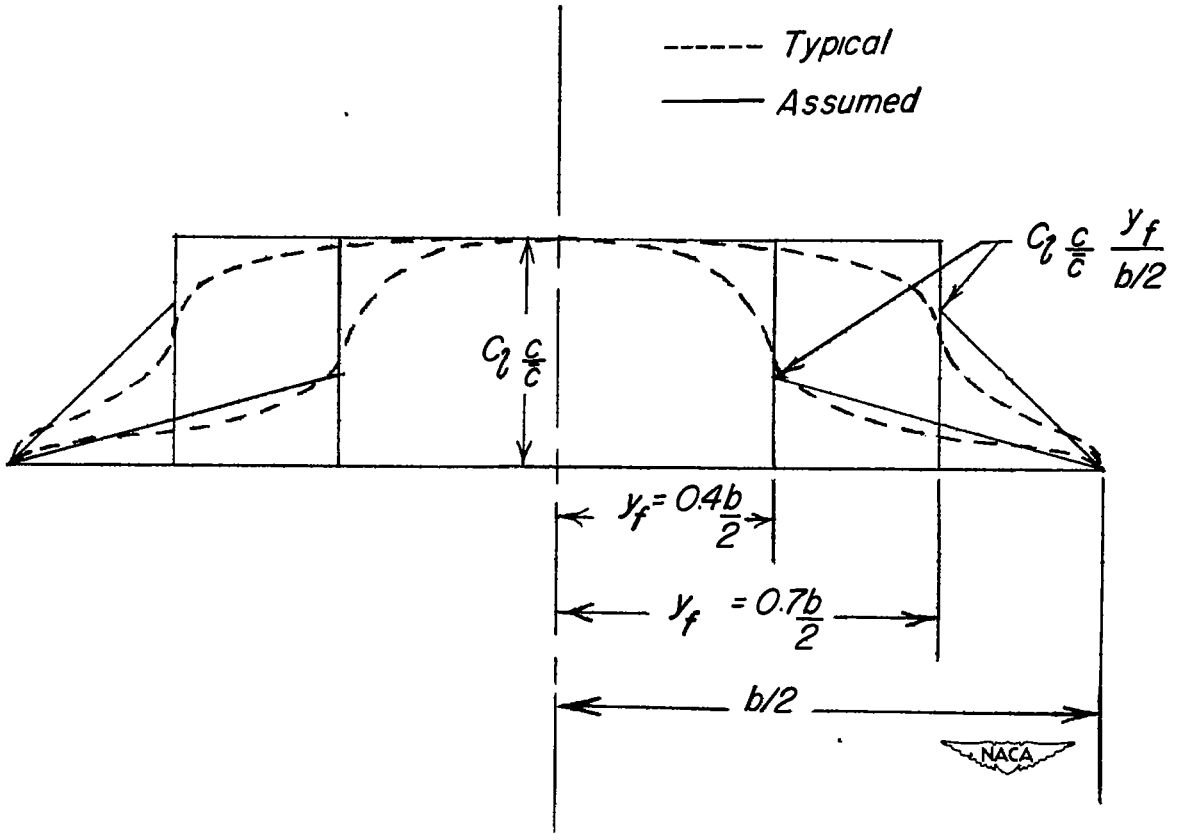

Figure 14.- Comparison of typical and assumed span loading over an untapered flapped wing. Assumed span loading was used in determining the spanwise center of pressure of the incremental flap load.

NACA-Langley - 11-7-52 - 1000